ELSEVIER

Contents lists available at ScienceDirect

Composite Structures

journal homepage: www.elsevier.com/locate/compstruct



Dual mesh control domain analysis of functionally graded circular plates accounting for moderate rotations



J.N. Reddy ^{a,*}, Praneeth Nampally ^a, Nam Phan ^b

- ^a Department of Mechanical Engineering, Texas A&M University, College Station, TX 77843-3123, USA
- ^b Structures Division, Naval Air Systems Command (NAVAIR), Patuxent River, MD 20670, USA

ARTICLE INFO

Keywords: Circular plates Classical and first-order shear deformation theories Functionally graded materials Mixed and displacement models Von Kármán nonlinearity The dual mesh control domain method

ABSTRACT

Nonlinear analysis of the axisymmetric bending of circular plates, accounting for through-thickness power-law variation of a two-constituent material and the von Kármán nonlinearity is presented using the dual mesh control domain methods (DMCDM). The classical and first-order shear deformation theory kinematics are used and displacement and mixed models are developed using the DMCDM. The DMCDM predicts displacements as accurate as the finite element method (FEM), but has the advantage of predicting the stress resultants more accurately than the FEM. The developed computational models are used to determine the effect of the geometric nonlinearity and power-law index on the bending deflections and stress resultants of functionally graded circular and annular plates with different boundary conditions. It is found that the power-law index, which dictates the material distribution through the thickness, has two different regions of response, one with steep increase in deflections followed by relatively slow increase with respect to the power-law index.

1. Background

1.1. Functionally graded materials

The last two decades have witnessed investigators exploring the possibility of using functionally graded materials (FGMs) as a promising alternative to conventional homogenous coatings (see Koizumi [1]). FGMs comprise of at least two constituents that are synthesized in such a way that the volume fractions of the constituents vary continuously along any desired spatial direction, resulting in materials having smooth variation of mechanical properties. Such property enhancements endow FGMs with material properties such as the resilience to fracture. FGMs promise attractive applications in a wide variety of wear coating and thermal shielding problems such as gears, cams, cutting tools, high temperature chambers, furnace liners, turbines, micro-electronics and space structures (see, e.g., Reddy and his colleagues [2-12] for the analysis of through-thickness, twoconstituent FGM beams and plates). The vast majority of twoconstituent FGM studies employed either a power-law or exponential distribution of the materials. In the power-law model, which is more commonly used in bending, vibration, and buckling studies, the modulus of elasticity E, for example, is assumed to vary through the thickness according to the formula (see [2])

$$E(z) = (E_1 - E_2)f(z) + E_2, \quad f(z) = \left(\frac{1}{2} + \frac{z}{h}\right)^n$$
 (1)

where E_1 and E_2 are the Youngs moduli of the top (material 1) and bottom (material 2) faces of the plate, respectively and n is the volume fraction exponent. The exponential model, which is often employed in fracture studies, is based on the formula (see [13,14])

$$E(z) = E_1 \exp\left[-\alpha \left(\frac{1}{2} - \frac{z}{h}\right)\right], \quad \alpha = \log\left(\frac{E_1}{E_2}\right)$$
 (2)

With the progress of technology and fast growth of the use of nanostructures, FGMs have found potential applications in micro and nano scales in the form of shape memory alloy thin films (see Lü et al. [15]), atomic force microscopes (AFMs) (see Kahrobaiyan et al. [16]), electrically actuated actuators (see Zhang and Fu [17]), and microswitches (see Shariat et al. [18]), to name a few. Arbind and Reddy [10] and Arbind, Reddy, and Srinivasa [11] accounted for the von Kármán nonlinear strains to develop nonlinear finite element models for functionally graded classical and first-order shear deformable beams. The von Kármán nonlinearity may have significant contribution to the response of micro- and nano-scale devices such as biosensors and atomic force microscopes (see, for example, Li et al. [19], and Pei et al. [20]).

E-mail addresses: jn reddy @ tamu.edu (J.N.~Reddy), praneeth.nampally @ tamu.edu (P.~Nampally), nam.phan @ navy.mil (N.~Phan).

^{*} Corresponding author.

1.2. The dual mesh control domain method

The finite element method (FEM) as an analysis tool has dominated the solid and structural mechanics field, while the finite volume method (FVM) witnessed tremendous growth and applications as applied to heat transfer and fluid mechanics fields. These methods are fundamentally different in arriving at the final discretized equations associated with a differential equation. The FEM is endowed with three basic features that no other method has (see Reddy [21]); (1) division of the domain into subdomains, called finite elements that allow unique derivation of interpolations functions used for the approximation of the geometry as well as the dependent unknowns, (2) derivation of the discretized equations, called the finite element model, over a typical element, using a method of approximation (e.g., Ritz, Galerkin, least-squares, subdomain, and so on; see Reddy [22]), and (3) assembly of the elements, using continuity and balance conditions, to obtain the discretized equations of the whole domain. We remark that families of interpolation functions on various geometries existed long before the FEM came into existence. Thus, calling these geometries as finite elements is appropriate only when they are used in the FEM; otherwise, they are just what they are geometrically - triangles, quadrilaterals, tetrahedrals, bricks, and so on. The FVM (see [23-25]) also represents the domain as a collection of subdomains with mesh points, and then a second mesh is placed over the first mesh such that the mesh points are in the interior of the second mesh. The subdomains of the second mesh are called control volumes, over which global form of the governing equations is satisfied. In the conventional FVM, the derivatives of the dependent variable at the interfaces of the control volumes are expressed in terms of the values of the variables at the mesh points using Taylor's series. In recent years, some FVM researchers have started using the first mesh to be one composed of triangles, rectangles, tetrahedrals, etc. In the FVM, the discretized equations consist of values of the unknowns at all mesh points connected to the control volume through the first mesh, resulting in a finite-difference-like stencil at the mesh point. The stencil is used repeatedly to obtain equations at all mesh points of the domain

Every engineering system has duality pairs – cause and effect, sometimes more than one pair, depending on the phenomena being modeled. Examples of the duality pairs are provided by (displacement, force) and (temperature, heat/flux). One must know one of the quantities of each pair at all mesh points (in some cases, a relation between them is known without having the knowledge of either quantity). In the FEM, the discretized equations often represent the algebraic relations among the nodal values of the duality pairs. Consequently, the imposition of boundary conditions in the FEM – whether one quantity or the other in the duality pair is known – are physical, and one does not replace the derivative at a boundary point in terms of the variable at the point. This concept of "duality" is not used in the FVM.

Recently, Reddy [26] introduced a numerical approach termed the dual mesh control domain method (DMCDM), previously called the dual mesh finite domain method, which utilizes the desirable features of the FEM and FVM. In the DMCDM, the domain is represented with a primal mesh of finite elements (i.e., define the approximations used for the unknowns), which allows a unique representation of the dependent unknowns, and a dual mesh is superimposed on the primal mesh such that the nodes of the primal mesh are in the interior of the dual mesh of control domains. Then the governing equation is satisfied in an integral sense over the control domain, similar to the FVM. The approach does not involve isolating a finite element domain and satisfying the governing equations in a weak sense over it and assembling element equations to obtain the global equations. Instead, the DMCDM results, much like in the FVM, directly in a set of global equations in terms of the nodal values of the primary variables. Thus, the DMCDM brings the desirable features of the FEM and the FVM, and comes closer to the FVM, where the first mesh is composed of the standard finite elements (geometry as well as approximation functions).

The major merits of the DMCDM are that the method inherits the desirable aspect of the FVM (in satisfying the global form of the governing equations over the control domains) and overcomes the disadvantage of the discontinuity of the secondary variables at the interfaces of the finite elements by calculating them at the boundaries of the control domains, where they are continuous (i.e., uniquely defined). The concept of duality and secondary variables are used to implement specified boundary conditions in the same way as in the FEM. The DMCDM has been domonstrated to yield accurate solutions for beams [27,28], axisymmetric circular plates [29], and heat transfer and fluid mechanics [30,31].

1.3. Present study

In the present study, the DMCDM has been extended to geometrically nonlinear analysis of axisymmetric bending of functionally graded circular and annular plates. Mixed formulation of the classical plate theory (CPT) and the displacement formulation of the first-order shear deformation plate theory (FSDT) are developed and their discretizations using the DMCDM are outlined. For comparison purposes, the mixed and displacement finite element models of the nonlinear bending of axisymetric circular plates are used, although their theoretical developments are not included here (see Reddy et al. [12] for the displacement model and [29] for the mixed model). These formulations account for through-thickness power-law variation of a twoconstituent material and the von Kármán nonlinear strains. Since nanoscale devices may involve circular plate elements that may be functionally graded and undergo moderately large rotations, the newly developed computational models can be used to determine response of circular plates. Moreover, the bending-extensional coupling is captured in the presence of the von Kármán nonlinear strains.

2. Governing equations

2.1. Preliminary comments

We consider a two-constituent functionally graded circular plate of outside radius R, inside radius a, and total thickness h. The r-coordinate is taken radially outward from the center the plate, z-coordinate along the thickness of the plate, and the θ -coordinate is taken along a circumference of the plate. We assume that the material of the plate is isotropic but varies from one kind of material at the bottom, z=-h/2, to another material at the top, z=h/2, so that the modulus E(z) of the material of the plate varies through the plate thickness according to the power-law in Eq. (1) (see Fig. 1). Poisson's ratio ν will be assumed to be constant throughout. When n=0, we obtain the single-material plate (with the property of material 1).

2.2. Classical plate theory

2.2.1. Displacement formulation

The equations of equilibrium of the CPT are (see Reddy [35,36])

$$\frac{1}{r} \left[-\frac{d}{dr} (rN_{rr}) + N_{\theta\theta} \right] = 0 \tag{3}$$

$$-\frac{1}{r}\frac{d}{dr}(rV_r) - q = 0 \tag{4}$$

where V_r is the effective transverse shear force acting on the rz-plane

$$V_{r} = \frac{1}{r} \left[\frac{d}{dr} (rM_{rr}) - M_{\theta\theta} + rN_{rr} \frac{dw}{dr} \right]$$
 (5)

and $N_{rr}, N_{\theta\theta}, M_{rr}$, and $M_{\theta\theta}$ are the stress resultants, which can be expressed in terms of the displacements (u, w) according to following the relations (assuming that Hooke's law holds)

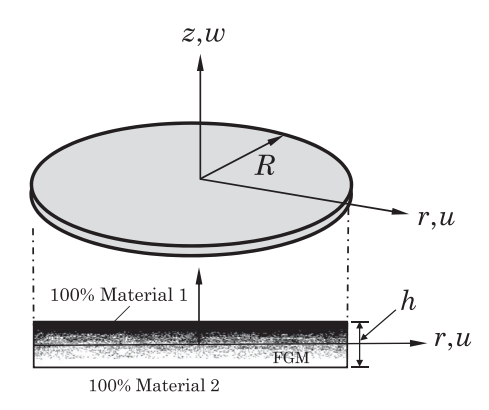


Fig. 1. Geometry and coordinate system for an axisymmetric bending of an FGM solid circular plate.

$$N_{rr} = \int_{-\frac{h}{2}}^{\frac{h}{2}} \sigma_{rr} dz = A \hat{\varepsilon}_{rr}^{(0)} + B \hat{\varepsilon}_{rr}^{(1)}$$
 (6a)

$$N_{\theta\theta} = \int_{-h}^{\frac{h}{2}} \sigma_{\theta\theta} dz = A \hat{\varepsilon}_{\theta\theta}^{(0)} + B \hat{\varepsilon}_{\theta\theta}^{(1)}$$
(6b)

$$M_{rr} = \int_{-\frac{L}{2}}^{\frac{L}{2}} \sigma_{rr} z \, dz = B \hat{\varepsilon}_{rr}^{(0)} + D \hat{\varepsilon}_{rr}^{(1)} \tag{6c}$$

$$\mathbf{M}_{\theta\theta} = \int_{-\frac{h}{2}}^{\frac{h}{2}} \sigma_{\theta\theta} \mathbf{z} \ d\mathbf{z} = B \hat{\varepsilon}_{\theta\theta}^{(0)} + D \hat{\varepsilon}_{\theta\theta}^{(1)}$$
(6d)

Here A, B, and D denote the extensional, extensional-bending, and bending stiffness of the plate:

$$(A,B,D) = \frac{1}{(1-\nu^2)} \int_{-\frac{h}{2}}^{\frac{h}{2}} E(z) (1,z,z^2) dz \tag{7}$$

and $\hat{\varepsilon}$ are the effective strains

$$\hat{\varepsilon}_{rr}^{(0)} = \left[\frac{du}{dr} + \frac{1}{2}\left(\frac{dw}{dr}\right)^2 + \nu\frac{u}{r}\right], \quad \hat{\varepsilon}_{rr}^{(1)} = -\left(\frac{d^2w}{dr^2} + \frac{\nu}{r}\frac{dw}{dr}\right) \tag{8a}$$

$$\hat{\varepsilon}_{\theta\theta}^{(0)} = \left[\frac{u}{r} + \nu \frac{du}{dr} + \frac{\nu}{2} \left(\frac{dw}{dr} \right)^2 \right], \quad \hat{\varepsilon}_{\theta\theta}^{(1)} = -\left(\nu \frac{d^2w}{dr^2} + \frac{1}{r} \frac{dw}{dr} \right)$$
(8b)

The boundary conditions of the CPT involve specifying one element of each of the following duality pairs:

$$(u, rN_{rr}), (w, rV_r), \left(-\frac{dw}{dr}, rM_{rr}\right)$$
 (9)

2.3. Mixed formulation

To reduce the order of the differential equations expressed in terms of the generalized displacements, from the fourth-order to the secondorder differential equations, in the case of the shear-constrained plate theory (i.e., classical plate theory), here we reformulate the governing equations of the classical plate theory as a set of second-order differential equations terms of the displacements (u, w) and the bending moment (M_{rr}) . Such formulations are known as *mixed* formulations (i.e., mixing displacement variables with force variables). Rewriting Eq. (8a) for the effective strains $\hat{\varepsilon}_{rr}^{(0)}$ and $\hat{\varepsilon}_{rr}^{(1)}$ and Eq. (8b) for the effective strains $\hat{\varepsilon}_{\theta\theta}^{(0)}$ and $\hat{\varepsilon}_{\theta\theta}^{(1)}$ in terms of the stress resultants N_r and M_r , we

$$\hat{\varepsilon}_{rr}^{(0)} = \frac{1}{D^*} (DN_{rr} - BM_{rr}), \quad \hat{\varepsilon}_{rr}^{(1)} = \frac{1}{D^*} (-BN_{rr} + AM_{rr})$$
 (10a)

$$\hat{\varepsilon}_{\theta\theta}^{(0)} = \frac{1}{D^*} (DN_{\theta\theta} - BM_{\theta\theta}), \quad \hat{\varepsilon}_{\theta\theta}^{(1)} = \frac{1}{D^*} (-BN_{\theta\theta} + AM_{\theta\theta})$$
 (10b)

A series of algebraic manipulations of Eqs. (10a) and (10b) to rewrite the stress resultants in terms of (u, w, M_r) results in

$$N_{rr} = \overline{A}\hat{\varepsilon}_{r}^{(0)} + \overline{B}M_{rr} = \overline{A}\left[\frac{du}{dr} + \frac{1}{2}\left(\frac{dw}{dr}\right)^{2} + \nu\frac{u}{r}\right] + \overline{B}M_{rr}$$
(11a)

$$M_{rr} = -D\left(\frac{d^2w}{dr^2} + \frac{\nu}{r}\frac{dw}{dr}\right) + D\overline{B}\left[\frac{du}{dr} + \frac{1}{2}\left(\frac{dw}{dr}\right)^2 + \nu\frac{u}{r}\right]$$
(11b)

$$M_{\theta\theta} = \nu M_{rr} + (1 - \nu^2) B \frac{u}{r} - (1 - \nu^2) D \frac{1}{r} \frac{dw}{dr}$$
 (11c)

$$N_{\theta\theta} = \overline{A} \left[\nu \frac{du}{dr} + \frac{1}{2} \nu \left(\frac{dw}{dr} \right)^2 + \frac{u}{r} \right] + \frac{1}{r} (1 - \nu^2) B \left(\overline{B}u - \frac{dw}{dr} \right) + \nu \overline{B}M_{rr} \quad (11d)$$

$$D^* = DA - B^2, \quad \overline{A} = \frac{D^*}{D} = A - B\overline{B}, \quad \overline{B} = \frac{B}{D}$$
 (12)

The two equilibrium equations, Eqs. (3) and (4), when N_{rr} , $N_{\theta\theta}$, and $M_{\theta\theta}$ are expressed in terms of u, w, and M_{rr} , along with Eq. (11b) provide the three required equations of the mixed formulation:

$$-\frac{1}{r}\frac{d}{dr}\left\{r\overline{A}\left[\frac{du}{dr} + \frac{1}{2}\left(\frac{dw}{dr}\right)^{2} + \nu\frac{u}{r}\right] + r\overline{B}M_{rr}\right\}$$

$$+\frac{1}{r}\overline{A}\left[\nu\frac{du}{dr} + \frac{\nu}{2}\left(\frac{dw}{dr}\right)^{2} + \frac{u}{r}\right] + \frac{1}{r}(1 - \nu^{2})B\left(\overline{B}\frac{u}{r} - \frac{1}{r}\frac{dw}{dr}\right) + \frac{1}{r}\nu\overline{B}M_{rr} = 0$$
(13)

$$-\frac{1}{r}\frac{d}{dr}\left[r\frac{dM_{rr}}{dr} + (1-\nu)M_{rr} - (1-\nu^{2})D\left(\overline{B}\frac{u}{r} - \frac{1}{r}\frac{dw}{dr}\right)\right]$$

$$-\frac{1}{r}\frac{d}{dr}\left\{r\overline{A}\left[\frac{dw}{dr}\frac{du}{dr} + \frac{1}{2}\left(\frac{dw}{dr}\right)^{3} + \nu\frac{dw}{dr}\frac{u}{r}\right] + r\overline{B}\frac{dw}{dr}M_{rr}\right\} - q = 0$$
(14)

$$-\frac{1}{r}\frac{d}{dr}\left(r\frac{dw}{dr}\right) + (1-\nu)\frac{1}{r}\frac{dw}{dr} + \overline{B}\left[\frac{du}{dr} + \frac{1}{2}\left(\frac{dw}{dr}\right)^{2} + \nu\frac{u}{r}\right] - \frac{1}{D}M_{rr} = 0$$
(15)

2.4. First-order shear deformation plate theory

The first-order shear deformation plate theory (FSDT) (see Reddy [35]) is the simplest theory that accounts for a nonzero transverse shear strain. The equations of equilibrium of the FSDT are

$$\frac{1}{r} \left[-\frac{d}{dr} (rN_{rr}) + N_{\theta\theta} \right] = 0 \tag{16}$$

$$-\frac{1}{r}\frac{d}{dr}(rV_r) - q = 0 \tag{17}$$

$$\frac{1}{r} \left[-\frac{d}{dr} (rN_{rr}) + N_{\theta\theta} \right] = 0$$

$$-\frac{1}{r} \frac{d}{dr} (rV_r) - q = 0$$

$$\frac{1}{r} \left[-\frac{d}{dr} (rM_{rr}) + M_{\theta\theta} \right] + Q_r = 0$$
(18)

The effective shear force V_r is defined by

$$V_r = Q_r + N_r \frac{dw}{dr} \tag{19}$$

and Q_r is shear stress resultant. The stress resultants in the first-order plate theory can be expressed in terms of the generalized displacements (u, w, ϕ) as

$$N_{rr} = \int_{-\frac{h}{2}}^{\frac{h}{2}} \sigma_{rr} dz = A \left[\frac{du}{dr} + \frac{1}{2} \left(\frac{dw}{dr} \right)^{2} + \nu \frac{u}{r} \right] + B \left(\frac{d\phi}{dr} + \frac{\nu}{r} \phi \right)$$

$$N_{\theta\theta} = \int_{-\frac{h}{2}}^{\frac{h}{2}} \sigma_{\theta\theta} dz = A \left[\frac{u}{r} + \nu \frac{du}{dr} + \frac{\nu}{2} \left(\frac{dw}{dr} \right)^{2} \right] + B \left(\nu \frac{d\phi}{dr} + \frac{1}{r} \phi \right)$$

$$M_{rr} = \int_{-\frac{h}{2}}^{\frac{h}{2}} \sigma_{rr} z dz = B \left[\frac{du}{dr} + \frac{1}{2} \left(\frac{dw}{dr} \right)^{2} + \nu \frac{u}{r} \right] + D \left(\frac{d\phi}{dr} + \frac{\nu}{r} \phi \right)$$

$$M_{\theta\theta} = \int_{-\frac{h}{2}}^{\frac{h}{2}} \sigma_{\theta\theta} z dz = B \left[\frac{u}{r} + \nu \frac{du}{dr} + \frac{\nu}{2} \left(\frac{dw}{dr} \right)^{2} \right] + D \left(\nu \frac{d\phi}{dr} + \frac{1}{r} \phi \right)$$

$$Q_{r} = K_{s} \int_{-\frac{h}{2}}^{\frac{h}{2}} \sigma_{rz} dz = S_{rz} \left(\phi + \frac{dw}{dr} \right)$$

where A, B, and D are the stiffnesses defined in Eq. (7), and S_{rz} is the shear stiffness

$$S_{rz} = \frac{K_s}{2(1+\nu)} \int_{-\frac{h}{2}}^{\frac{h}{2}} E(z) dz$$
 (21)

The boundary conditions involve specifying one element of each of the following duality pairs:

$$(u, rN_r), (w, rV_r), (\phi, rM_r)$$
 (22)

3. The dual mesh control domain models

3.1. Introduction

The displacement and mixed finite element models of CPT and the displacement model of the FSDT can be found in [28,29]. Therefore, these models are not discussed here. Instead, a detailed discussion of the DMCDM is presented.

Reddy [26] introduced a numerical approach termed the dual mesh finite domain method, which uses ideas from both the FEM and FVM to solve second-order equations (thus, higher-order equations must be expressed as a system of first- and second-order equations). In the DMCDM, the domain is represented with a primal mesh of finite elements, and a dual mesh is superimposed on the primal mesh such that the nodes of the primal mesh are inside the dual mesh (if the mesh is uniform, they will be at the center of the control domains) of finite/control domains, except for the nodes on the boundary. Then the governing equation is required to be satisfied in an integral sense (not in a weighted-integral sense, [35]) over the finite domain. The secondorder terms in the differential equation are integrated by parts and expressed as dual variables on the interfaces of the dual mesh. When the interfaces fall on the boundary, either the dual variables or their counterparts (i.e., primary variables) are known and thereby the derivatives are not replaced at the boundary nodes, eliminating the need for the so-called zero-thickness control volumes or fictitious control volumes. The DMCDM brings the best features of the FEM, namely, the interpolation of the variables and imposition of physical boundary conditions, and of the FVM in satisfying the actual balance equations over the control domain. The major merits of the DMCDM are that the method inherits the desirable aspect of the FVM (in satisfying the global form of the governing equations over the finite domains) and overcomes the disadvantage of the discontinuity of the secondary variables at the interfaces of the finite elements by calculating them at the boundaries of the control domains, where they are continuous (i.e., uniquely defined).

In the following discussion, we consider circular plates with axisymmetric conditions (i.e., material properties, boundary conditions, and loads are independent of the circumferential coordinate). Consequently, we can use any radial line as the domain of any circular plate problem (see Fig. 2). The domain is divided into a set of N nonoverlapping but connected subintervals, which we term "finite elements" (i.e., line elements with interpolation functions), much like in the finite element method (but we do not use the finite element method to obtain the discretized equations). This mesh of finite elements will be called the primal mesh. The connecting points of the primal mesh will be termed "nodes." For now, we assume that each element has two nodes (i.e., linear approximation), positioned at the ends of the line element. Then, we identify a second mesh, called the dual mesh, of line elements which covers the whole domain and bisect the elements of the primal mesh on either side of the nodes (i.e., the interfaces of the line elements of the dual mesh are at the center of the finite elements of the primal mesh), as shown in Fig. 2. The line elements of the dual mesh are called *control domains*. Every control domain contains a node of the primal mesh. We then isolate a typical line element of the dual mesh and satisfy the integral statements of the

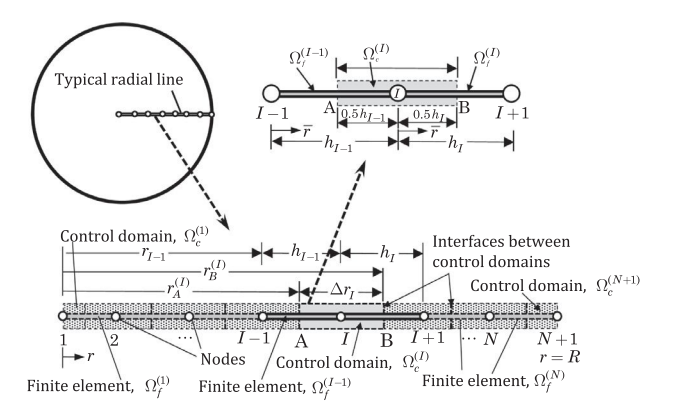


Fig. 2. A primal mesh of finite elements and dual mesh of control domains shown for a typical radial line of a circular plate. The *I*th finite element is denoted by $\Omega_f^{(I)}$. We note that the boundary nodes have only half control domains whereas the internal nodes have full control domains. Also, each control domain connects two neighboring finite elements, one on the left and the other on the right. The *I*th control domain, which houses the *I*th node, is denoted by $\Omega_c^{(I)}$. The control domain $\Omega_c^{(I)}$ associated with an interior node *I* is isolated to discuss the discretization. Every interior control domain connects three nodes (nine nodal degrees of freedom) through the discretization of the governing equation, whereas the boundary nodes connect two adjacent nodes.

governing equations. Since the control domain spans two adjacent elements, the satisfaction of the governing equations automatically relates the nodal values of the dependent unknowns at three consecutive nodes.

In the following subsections, we detail the discretization process for the mixed model of the CPT and the displacement model of the FSDT. For the purpose of readily seeing the meaning of the dual variables, we write the governing equations in terms of the strains $\hat{\varepsilon}_{rr}^{(0)},\hat{\varepsilon}_{\theta\theta}^{(0)},\hat{\varepsilon}_{\theta\theta}^{(1)}$, and M_{rr} . Ultimately, all equations expressed in terms of the unknowns of the model and the unknowns are approximated using linear finite element interpolation functions. For example, a typical unknown u is approximated over a typical finite element $\Omega_f^{(J)}=(r_J,r_{J+1})$ (the element $\Omega_f^{(J)}$ is on the right side of the node J) by

$$u(r) \approx U_J \psi_1^{(J)}(r) + U_{J+1} \psi_2^{(J)}(r) \tag{23}$$

where U_J is the value of u at node J (i.e., $U_J \approx u(r_J)$) and $\psi_i^{(J)}(r)$ (i=1,2) are linear finite element interpolation functions of element $\Omega_f^{(J)}$ for $J=1,2,\ldots,N$, expressed in terms of the coordinate r (r has its origin at the center of the plate):

$$\psi_1^{(J)}(r) = \frac{r_{J+1} - r}{h_J}, \quad \psi_2^{(J)}(r) = \frac{r - r_J}{h_J}$$
 (24)

Similar approximations are used for other dependent unknowns. When the integral statements are evaluated at a boundary node, either the secondary variable or the corresponding primary variable is known at the node and, therefore, one need not express the secondary variables in terms of the gradients of the primary variables and approximate them in terms of the nodal values of the primary variables. In the interior of the domain, the secondary variables appearing in the integral statements for an interior node I are replaced in terms of the nodal values of the dependent unknowns using the finite element approximation of the form in Eq. (23), while linearizing the nonlinear terms. In this study, we assume that all of the stiffness coefficients A, B, and D are constant (i.e., independent of position). The details are presented next.

3.2. Mixed model of the CPT

The dual mesh finite domain statements of Eqs. (13)–(15) are obtained as follows:

$$0 = -\int_{r_{A}^{(J)}}^{r_{B}^{(J)}} \frac{1}{r} \left[\frac{d}{dr} \left(r \overline{A} \hat{\varepsilon}_{rr}^{(0)} + r \overline{B} M_{rr} \right) - A \hat{\varepsilon}_{\theta\theta}^{(0)} - B \hat{\varepsilon}_{\theta\theta}^{(1)} \right] r dr$$

$$= -\left[r \overline{A} \hat{\varepsilon}_{rr}^{(0)} + r \overline{B} M_{rr} \right]_{r_{A}^{(J)}}^{r_{B}^{(J)}} - \int_{r_{A}^{(J)}}^{r_{B}^{(J)}} \left(A \hat{\varepsilon}_{\theta\theta}^{(0)} + B \hat{\varepsilon}_{\theta\theta}^{(1)} \right) dr = -N_{1}^{(J)} - N_{2}^{(J)}$$

$$- \int_{r_{A}^{(J)}}^{r_{B}^{(J)}} \left(A \hat{\varepsilon}_{\theta\theta}^{(0)} + B \hat{\varepsilon}_{\theta\theta}^{(1)} \right) dr$$
(25)

$$\begin{split} 0 &= -\int_{r_{A}^{(J)}}^{r_{B}^{(J)}} \left\{ \frac{1}{r} \frac{d}{dr} \left[\frac{d}{dr} (rM_{rr}) - B \hat{\varepsilon}_{\theta\theta}^{(0)} - D \hat{\varepsilon}_{\theta\theta}^{(1)} + \overline{A} r \frac{dw}{dr} \hat{\varepsilon}_{rr}^{(0)} + \overline{B} r \frac{dw}{dr} M_{rr} \right] + q \right\} r dr \\ &= -\left[\frac{d}{dr} (rM_{rr}) - B \hat{\varepsilon}_{\theta\theta}^{(0)} - D \hat{\varepsilon}_{\theta\theta}^{(1)} + \overline{A} r \frac{dw}{dr} \hat{\varepsilon}_{rr}^{(0)} + \overline{B} r \frac{dw}{dr} M_{rr} \right]_{r_{A}^{(J)}}^{r_{B}^{(J)}} \\ &- \int_{r_{A}^{(J)}}^{r_{B}^{(J)}} q r dr = -V_{1}^{(J)} - V_{2}^{(J)} - \int_{r_{A}^{(J)}}^{r_{B}^{(J)}} q r dr \end{split}$$

$$(26)$$

$$\begin{split} 0 &= \int_{r_A^{(J)}}^{r_B^{(J)}} \left\{ -\frac{1}{r} \frac{d}{dr} \left(r \frac{dw}{dr} \right) + (1 - \nu) \frac{1}{r} \frac{dw}{dr} + \bar{B} \left[\frac{du}{dr} + \frac{1}{2} \left(\frac{dw}{dr} \right)^2 + \nu \frac{u}{r} \right] - \frac{1}{D} M_{rr} \right\} r dr \\ &= -\left[r \frac{dw}{dr} \right]_{r_A^{(J)}}^{r_B^{(J)}} + \int_{r_A^{(J)}}^{r_B^{(J)}} \left\{ (1 - \nu) \frac{dw}{dr} + r \bar{B} \left[\frac{du}{dr} + \frac{1}{2} \left(\frac{dw}{dr} \right)^2 + \nu u \right] - \frac{r}{D} M_{rr} \right\} dr \\ &= -\Theta_1^{(J)} - \Theta_2^{(J)} + \int_{r_A^{(J)}}^{r_B^{(J)}} \left\{ (1 - \nu) \frac{dw}{dr} + r \bar{B} \left[\frac{du}{dr} + \frac{1}{2} \left(\frac{dw}{dr} \right)^2 + \nu u \right] - \frac{r}{D} M_{rr} \right\} dr \end{split}$$

where the secondary variables N, V, and Θ are defined by

$$N_1^{(J)} = -(rN_r)|_{r^{(J)}}, N_2^{(J)} = (rN_r)|_{r^{(J)}}$$
(28a)

$$V_1^{(J)} = -(rV_r)|_{r^{(J)}}, V_2^{(J)} = (rV_r)|_{r^{(J)}}$$
(28b)

$$\Theta_{1}^{(J)} = -\left(r\frac{dw}{dr}\right)|_{r_{A}^{(J)}}, \Theta_{2}^{(J)} = \left(r\frac{dw}{dr}\right)|_{r_{B}^{(J)}}$$
(28c)

For a typical interior node I, the secondary variables in Eqs. (28a)–(28c) can be expressed in terms of the nodal values of u, w, and M:

$$egin{aligned} N_1^{(I)} &= -\overline{A} \left(r_A^{(I)} rac{U_I - U_{I-1}}{h_{I-1}} + 0.5 r_A^{(I)} \, \delta W_{I-1} rac{W_I - W_{I-1}}{h_{I-1}} +
u rac{U_I + U_{I-1}}{2}
ight) \ &- r_A^{(I)} \, \overline{B} rac{M_I + M_{I-1}}{2} \end{aligned}$$

$$egin{split} N_{2}^{(I)} &= \overline{A} igg(r_{B}^{(I)} rac{U_{I+1} - U_{I}}{h_{I}} + 0.5 r_{B}^{(I)} \, \delta W_{I} rac{W_{I+1} - W_{I}}{h_{I}} +
u rac{U_{I+1} + U_{I}}{2} igg) \ &+ r_{B}^{(I)} \overline{B} rac{M_{I+1} + M_{I}}{2} \end{split}$$

$$\begin{split} V_{1}^{(I)} &= -\left[r_{A}^{(I)}\frac{M_{I}-M_{I-1}}{h_{I-1}} + (1-\nu)\frac{M_{I}+M_{I-1}}{2} + r_{A}^{(I)}\overline{B}\,\delta W_{I-1}\frac{M_{I}+M_{I-1}}{2} \right. \\ &\left. - \left(1-\nu^{2}\right)D\left(\overline{B}\frac{U_{I}+U_{I-1}}{2r_{A}^{(I)}} - \frac{W_{I}-W_{I-1}}{h_{I-1}}r_{A}^{(I)}\right)\right] \\ &\left. - \overline{A}\,\delta W_{I-1}\left(r_{A}^{(I)}\frac{U_{I}-U_{I-1}}{h_{I-1}} + 0.5r_{A}^{(I)}\,\delta W_{I-1}\frac{W_{I}-W_{I-1}}{h_{I-1}} + \nu\frac{U_{I}+U_{I-1}}{2}\right) \right. \end{split}$$

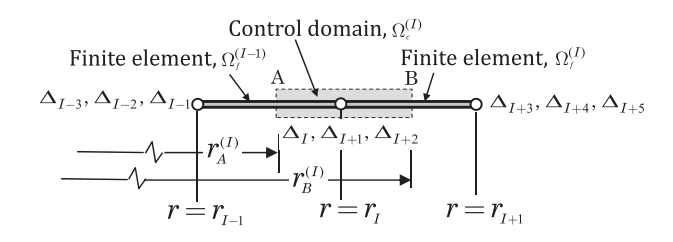


Fig. 3. The control domain $\Omega_c^{(I)}$ associated with an interior node I, the nodal coordinates, coordinates of the control volume interfaces, and the nodal degrees of freedom (3 degrees of freedom per node).

$$\begin{split} V_{2}^{(I)} &= \left[r_{B}^{(I)} \frac{M_{I+1} - M_{I}}{h_{I}} + (1 - \nu) \frac{M_{I+1} + M_{I}}{2} \right. \\ &- \left. (1 - \nu^{2}) D \left(\overline{B} \frac{U_{I+1} + U_{I}}{2 r_{B}^{(I)}} - \frac{W_{I+1} - W_{I}}{h_{I} r_{B}^{(I)}} \right) \right] \\ &+ \overline{A} \, \delta W_{I} \left(r_{B}^{(I)} \frac{U_{I+1} - U_{I}}{h_{I}} + 0.5 r_{B}^{(I)} \, \delta W_{I} \frac{W_{I+1} - W_{I}}{h_{I}} + \nu \frac{U_{I+1} + U_{I}}{2} \right) \\ &+ r_{B}^{(I)} \, \overline{B} \, \delta W_{I} \frac{M_{I+1} + M_{I}}{2} \\ \Theta_{1}^{(I)} &= -r_{A}^{(I)} \frac{W_{I} - W_{I-1}}{h_{I-1}}, \quad \Theta_{2}^{(I)} &= r_{B}^{(I)} \frac{W_{I+1} - W_{I}}{h_{I}} \end{split}$$

where the superscript (I) refers to the control domain $\Omega_c^{(I)}$, the subscript I refers to the element number $\Omega_f^{(I)}$ (the control domain $\Omega_c^{(I)}$ partially occupies finite element $\Omega_f^{(I-1)}$ on the left and finite element $\Omega_f^{(I)}$ on the right), and

$$\delta W_{I-1} = \frac{\overline{W}_I - \overline{W}_{I-1}}{h_{I-1}}, \quad \delta W_I = \frac{\overline{W}_{I+1} - \overline{W}_I}{h_I}$$
 (29f)

and \overline{W}_{I-1} and \overline{W}_I are the nodal value of w from the previous iteration. To obtain the discretized equations associated with Eqs. (25)–(27), we use the relations in Eqs. (29a)–(29e). With the relations in Eqs. (51a)-(51j), the discretized form of Eqs. (25)–(27) can be expressed in the form (we note that these are global equations and contain coefficients of nine variables associated with three consecutive nodes; the number of degrees of freedom per node is 3):

$$\begin{aligned} 0 &= K_{I-3}^{I} \Delta_{I-3} + K_{I}^{I} \Delta_{I} + K_{I+3}^{I} \Delta_{I+3} + K_{I-2}^{I} \Delta_{I-2} + K_{I+1}^{I} \Delta_{I+1} \\ &+ K_{I+4}^{I} \Delta_{I+4} + K_{I-1}^{I} \Delta_{I-1} + K_{I+2}^{I} \Delta_{I+2} + K_{I+5}^{I} \Delta_{I+5} \end{aligned}$$

$$(30)$$

$$0 &= K_{I-3}^{I+1} \Delta_{I-3} + K_{I}^{I+1} \Delta_{I} + K_{I+3}^{I+1} \Delta_{I+3} + K_{I-2}^{I+1} \Delta_{I-2} + K_{I+1}^{I+1} \Delta_{I+1} \\ &+ K_{I+4}^{I+1} \Delta_{I+4} + K_{I-1}^{I+1} \Delta_{I-1} + K_{I+2}^{I+1} \Delta_{I+2} + K_{I+5}^{I+1} \Delta_{I+5} - F_{I+1}^{I+1} \\ 0 &= K_{I-3}^{I+2} \Delta_{I-3} + K_{I}^{I+2} \Delta_{I} + K_{I+3}^{I+2} \Delta_{I+3} + K_{I-2}^{I+2} \Delta_{I-2} + K_{I+1}^{I+2} \Delta_{I+1} \\ &+ K_{I+4}^{I+2} \Delta_{I+4} + K_{I-1}^{I+2} \Delta_{I-1} + K_{I+2}^{I+2} \Delta_{I+2} + K_{I+5}^{I+2} \Delta_{I+5} \end{aligned}$$

$$(32)$$

for I = 4, 7, 10, ..., 3N, where N is the number of elements (or N + 1 is the number of nodes) in the mesh. Here Δ is the vector of global primary degrees of freedom (see Fig. 3):

$$\Delta_{I-3} = U_{J-1}, \quad \Delta_{I} = U_{J}, \quad \Delta_{I+3} = U_{J+1}
\Delta_{I-2} = W_{J-1}, \quad \Delta_{I+1} = W_{J}, \quad \Delta_{I+4} = W_{J+1}
\Delta_{I-1} = M_{J-1}, \quad \Delta_{I+2} = M_{J}, \quad \Delta_{I+5} = M_{J+1}$$
(33)

and $K_K^I = K_{IK}$ are the stiffness coefficients presented in Appendix A.1 [see Eqs. (13)–(15)]. For boundary node 1, the discretized equations are

$$0 = -N_1^{(1)} + K_1^1 \Delta_1 + K_4^1 \Delta_4 + K_2^1 \Delta_2 + K_5^1 \Delta_5 + K_3^1 \Delta_3 + K_6^1 \Delta_6$$
 (34)

$$0 = -V_1^{(1)} + K_1^2 \Delta_1 + K_2^2 \Delta_4 + K_2^2 \Delta_2 + K_5^2 \Delta_5 + K_2^2 \Delta_3 + K_6^2 \Delta_6 - F^2$$
 (35)

$$0 = -\Theta_1^{(1)} + K_1^3 \Delta_1 + K_2^3 \Delta_4 + K_2^3 \Delta_2 + K_5^3 \Delta_5 + K_3^3 \Delta_3 + K_6^3 \Delta_6$$
 (36)

(29a)

(29b)

where the coefficients K^I_J are defined in Appendix B.1. Similar relations can be written for node N+1.

3.3. Displacement model of the FSDT

The dual mesh finite domain statements of Eqs. (16)–(18), with the stress resultants defined by Eq. (20), are obtained as follows:

$$0 = \int_{r_{s}^{(J)}}^{r_{B}^{(J)}} \left\{ \frac{1}{r} \left[-\frac{d}{dr} (rN_{rr}) + N_{\theta\theta} \right] \right\} r dr = -N_{1}^{(J)} - N_{2}^{(J)} + \int_{r_{s}^{(J)}}^{r_{B}^{(J)}} N_{\theta\theta} dr \quad (37)$$

$$0 = \int_{r^{(J)}}^{r_B^{(J)}} \left[-\frac{1}{r} \frac{d}{dr} (rV_r) - q \right] r dr = -V_1^{(J)} - V_2^{(J)} - \int_{r^{(J)}}^{r_B^{(J)}} r q(r) dr$$
 (38)

$$0 = \int_{r_A^{(J)}}^{r_B^{(J)}} \left\{ \frac{1}{r} \left[-\frac{d}{dr} (rM_{rr}) + M_{\theta\theta} \right] + Q_r \right\} r dr = -M_1^{(J)} - M_2^{(J)} + \int_{r_B^{(J)}}^{r_B^{(J)}} (M_{\theta\theta} + rQ_r) dr$$
(39)

where the secondary variables N, V, and M are defined by

$$N_1^{(J)} = -(rN_r)|_{r^{(J)}}, \quad N_2^{(J)} = (rN_r)|_{r^{(J)}}$$
 (40a)

$$V_1^{(J)} = -(rV_r)|_{r^{(J)}}, \quad V_2^{(J)} = (rV_r)|_{r^{(J)}}$$
 (40b)

$$M_1^{(J)} = -(rM_r)|_{r^{(J)}}, \quad M_2^{(J)} = (rM_r)|_{r^{(J)}}$$
 (40c)

For a typical interior node *I*, the secondary variables in Eqs. (40a)–(40c) can be expressed in terms of the nodal values of u, w, and ϕ :

$$\begin{split} N_{1}^{(I)} &= -A \left(r_{A}^{(I)} \frac{U_{I} - U_{I-1}}{h_{I-1}} + 0.5 r_{A}^{(I)} \, \delta W_{I-1} \frac{W_{I} - W_{I-1}}{h_{I-1}} + \nu \frac{U_{I} + U_{I-1}}{2} \right) \\ &- B \left(r_{A}^{(I)} \frac{\Phi_{I} - \Phi_{I-1}}{h_{I-1}} + \nu \frac{\Phi_{I} + \Phi_{I-1}}{2} \right) \\ N_{2}^{(I)} &= A \left(r_{B}^{(I)} \frac{U_{I+1} - U_{I}}{h_{I}} + 0.5 r_{B}^{(I)} \, \delta W_{I} \frac{W_{I+1} - W_{I}}{h_{I}} + \nu \frac{U_{I+1} + U_{I}}{2} \right) \\ &+ B \left(r_{B}^{(I)} \frac{\Phi_{I+1} - \Phi_{I}}{h_{I}} + \nu \frac{\Phi_{I+1} + \Phi_{I}}{2} \right) \end{split} \tag{41b}$$

$$V_{1}^{(I)} = -\left\{r_{A}^{(I)}S_{rz}\left(\frac{\Phi_{I} + \Phi_{I-1}}{2} + \frac{W_{I} - W_{I-1}}{h_{I-1}}\right) + \delta W_{I-1}\left[r_{A}^{(I)}\frac{U_{I} - U_{I-1}}{h_{I-1}} + 0.5r_{A}^{(I)}\delta W_{I-1}\frac{W_{I} - W_{I-1}}{h_{I-1}} + \nu\frac{U_{I} + U_{I-1}}{2}\right] + B\delta W_{I-1}\left(r_{A}^{(I)}\frac{\Phi_{I} - \Phi_{I-1}}{h_{I-1}} + \nu\frac{\Phi_{I} + \Phi_{I-1}}{2}\right)\right\}$$
(41c)

$$\begin{split} V_{2}^{(I)} &= \left\{ r_{B}^{(I)} S_{rz} \left(\frac{\Phi_{I} + \Phi_{I+1}}{2} + \frac{W_{I+1} - W_{I}}{h_{I}} \right) \right. \\ &+ A \delta W_{I} \left[r_{B}^{(I)} \frac{U_{I+1} - U_{I}}{h_{I}} + 0.5 r_{B}^{(I)} \delta W_{I} \frac{W_{I+1} - W_{I}}{h_{I}} + \nu \frac{U_{I} + U_{I+1}}{2} \right] \\ &+ B \delta W_{I} \left(r_{B}^{(I)} \frac{\Phi_{I+1} - \Phi_{I}}{h_{I}} + \nu \frac{\Phi_{I} + \Phi_{I+1}}{2} \right) \right\} & (41d) \\ M_{1}^{(I)} &= -B \left(r_{A}^{(I)} \frac{U_{I} - U_{I-1}}{h_{I-1}} + 0.5 r_{A}^{(I)} \delta W_{I-1} \frac{W_{I} - W_{I-1}}{h_{I-1}} + \nu \frac{U_{I} + U_{I-1}}{2} \right) \\ &- D \left(r_{A}^{(I)} \frac{\Phi_{I} - \Phi_{I-1}}{h_{I-1}} + \nu \frac{\Phi_{I} + \Phi_{I-1}}{2} \right) & (41e) \\ M_{2}^{(I)} &= B \left(r_{B}^{(I)} \frac{U_{I+1} - U_{I}}{h_{I}} + 0.5 r_{B}^{(I)} \delta W_{I} \frac{W_{I+1} - W_{I}}{h_{I}} + \nu \frac{U_{I+1} + U_{I}}{2} \right) \\ &+ D \left(r_{B}^{(I)} \frac{\Phi_{I+1} - \Phi_{I}}{h_{I}} + \nu \frac{\Phi_{I+1} + \Phi_{I}}{2} \right) & (41f) \end{split}$$

The discretized form of Eqs. (37)–(39) can be expressed in the same form as Eqs. (30)–(32), with Δ defined by

$$\Delta_{I-3} = U_{J-1}, \quad \Delta_{I} = U_{J}, \quad \Delta_{I+3} = U_{J+1}
\Delta_{I-2} = W_{J-1}, \quad \Delta_{I+1} = W_{J}, \quad \Delta_{I+4} = W_{J+1}
\Delta_{I-1} = \Phi_{J-1}, \quad \Delta_{I+2} = \Phi_{J}, \quad \Delta_{I+5} = \Phi_{J+1}$$
(42)

The coefficients $K_K^I = K_{IK}$ for this model are defined in Appendix A.2. For boundary node 1, the discretized equations are

$$0 = -N_1^{(1)} + K_1^1 \Delta_1 + K_4^1 \Delta_4 + K_2^1 \Delta_2 + K_5^1 \Delta_5 + K_2^1 \Delta_3 + K_6^1 \Delta_6 \tag{43}$$

$$0 = -V_1^{(1)} + K_1^2 \Delta_1 + K_2^2 \Delta_4 + K_2^2 \Delta_2 + K_5^2 \Delta_5 + K_2^2 \Delta_3 + K_6^2 \Delta_6 - F^2$$
 (44)

$$0 = -M_1^{(1)} + K_1^3 \Delta_1 + K_2^3 \Delta_2 + K_2^3 \Delta_2 + K_3^3 \Delta_5 + K_2^3 \Delta_3 + K_6^3 \Delta_6 \tag{45}$$

where K^I_J are defined in Appendix B.2. Similar expressions can be written for node N+1.

4. Numerical results

Here we present numerical results obtained with various finite element (FEM) and dual mesh control domain (DMCDM) models developed in the preceding sections. Numerical results obtained with the FEM and DMCDM are compared in all cases. We use three models of the FEM and two models of the DMFDM, as designated here:

- FE-CP(D) Displacement finite element model of the CPT
- FE-CP(M) Mixed finite element model of the CPT
- FE-FS(D) Displacement finite element model of the FSDT
- DM-CP(M) Mixed dual mesh finite domain model of the CPT
- DM-FS(D) Displacement dual mesh finite domain model of the FSDT

The FE-CP(D) model uses Hermite cubic interpolation of w(r) and linear interpolation of u(r), whereas all other elements are based on Lagrange interpolations of all variables. All finite element models other than FE-CP(D) can also use quadratic or higher order interpolations, whereas the dual mesh control domain formulations presented herein are based on linear interpolations. Thus, for consistency, all numerical results presented herein, with the exception of FE-CP(D), are obtained with linear approximations of all field variables. In obtaining the numerical solutions, we shall consider functionally graded circular plates of radius R=10 in (25.4 cm) and thickness h=0.1 in (0.254 cm), and subjected to uniformly distributed load of intensity q_0 lb/in (1 lb/in = 175 N/m). The FGM beam is made of two materials with the following values of the moduli, Poisson's ratio, and shear correction coefficient:

$$E_1 = 30 \times 10^6 \; \mathrm{psi}(207 \; \mathrm{GPa}), \quad E_2 = 3 \times 10^6 \; \mathrm{psi}(21 \; \mathrm{GPa}), \quad \nu = 0.3,$$

$$K_s = \frac{5}{6}$$

We shall investigate the parametric effects of the power-law index, n, and boundary conditions on the linear and nonlinear transverse deflections and bending moments.

4.1. Linear analysis

Here we consider functionally graded circular plates which are either pinned or clamped at the (outer) edge. The boundary conditions on the primary variables $(M=M_{rr})$ in various models for the pinned case are as follows:

Displacement
models :
$$u(0)=0$$
, and $\frac{dw}{dr}=0$ or $\phi(0)=0$ at $r=0$;
 $u(R)=w(R)=0$ (46a)

Mixedmodels:
$$u(0) = 0$$
, $u(R) = w(R) = M(R) = 0$ (46b)

The exact solution for the transverse deflection of pinned functionally graded circular plates according to the FSDT, with the power-law given in Eq. (1) $[B \neq 0; D^* = DA - B^2;$ see Eqs. (7) and (12)], are given by (see [34,33])

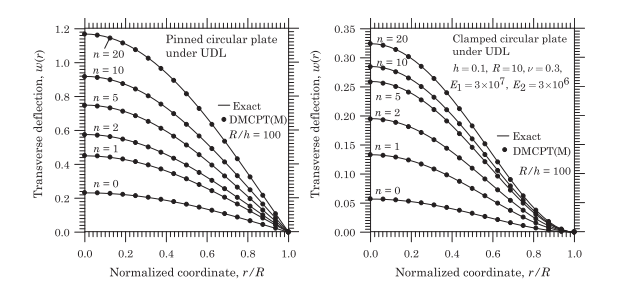


Fig. 4. Plots of the center deflection of pinned circular plates as functions of the normalized radial coordinate, r/R, for various value of the power-law index, n. The solid lines correspond to the analytical solutions and symbols to the numerical solutions.

$$u(r) = \frac{Bq_0R^3}{16D^*} \left(-\xi + \xi^3 \right) \tag{47a}$$

$$\begin{split} u(r) &= \frac{Bq_0R^3}{16D^*} \left(-\xi + \xi^3 \right) \\ w(r) &= \frac{Aq_0R^4}{64D^*} \left[\xi^4 - 2\left(\frac{3+\nu}{1+\nu} \right) \xi^2 + \frac{5+\nu}{1+\nu} + \frac{4B^2}{DA(1+\nu)} \left(\xi^2 - 1 \right) \right] + \frac{q_0R^2}{4S_{rs}} \left(1 - \xi^2 \right) \end{split}$$

$$\phi(r) = \frac{Aq_0R^3}{16D^*} \left[-\frac{2B^2}{DA(1+\nu)} \xi + \frac{(3+\nu)}{(1+\nu)} \xi - \xi^3 \right]$$
(47c)

$$M_{rr}(r) = \frac{(3+\nu)q_0R^2}{16} (1-\xi^2) \tag{47d}$$

where $\xi = r/R$. The CPT solutions are given by setting $1/S_{rz}$ to zero, and the solutions for homogeneous plates are obtained by setting B = 0.

The boundary conditions on the primary variables in various models for the clamped circular plate are as follows (replace dw/dr with ϕ for the FSDT):

Displacement models:
$$u(0)=0, \quad \frac{dw}{dr}(0)=0, \quad u(R)=w(R)=\frac{dw}{dr}(R)=0$$
 (48a)

Mixedmodels:
$$u(0) = 0$$
, $u(R) = w(R) = 0$ (48b)

The exact solution for the transverse deflection of functionally graded clamped circular plate according to the FSDT is

$$u(r) = \frac{Bq_0R^3}{16D^*} \left(-\xi + \xi^3 \right) \tag{49a}$$

$$w(r) = \frac{Aq_0R^4}{64D^*} (1 - \xi^2)^2 + \frac{q_0R^2}{4S_{rz}} (1 - \xi^2)$$
(49b)

$$\phi(r) = \frac{Aq_0R^3}{16D^*} (\xi - \xi^3) \tag{49c}$$

$$M_{rr}(r) = \frac{q_0 R^2}{16} \left[(1 + \nu) - (3 + \nu) \xi^2 \right]$$
 (49d)

Extensive numerical studies have been carried out with various models (also see [29]), including mesh Independence and value of the acceleration parameter on the nonlinear convergence, effect of the power-law index, and post-computation of the stress resultants (either the bending moments or the rotations). In all cases, both the DMCDM and FEM models, using 16 linear elements, yield results that are indistinguishable in a graphical presentations. Most interestingly, it is found that the post-computed rotations (in mixed models) and bending moments (in displacement models) are very accurate (one cannot distinguish between the exact and numerical solutions), except at r = 0. Based on the numerical studies, the following observations are made concerning the linear solutions.

(1) The nodal generalized displacements predicted by FE-CP(D) match the exact CPT solutions for the pinned and clamped plates. (2) The post-computed shear forces in DM-FS(D) and DM-CP(M) match the exact solution for the pinned and clamped plates.

Fig. 4 contains plots of the deflections w(0) predicted for the pinned plates and clamped plates as a function of the normalized radial coordinate, r/R. The deflections predicted (shown by symbols) by all FEM and DMCDM models are essentially the same (i.e., the differences cannot be seen in the graph) and match with the analytical solutions (shown as lines); this also indicates that the effect of shear deformation is negligible (because R/h = 100, a thin plate). The post-computed and nodal values of the bending moment M_{rr} are plotted as functions of the normalized radial coordinate, r/R in Fig. 5. Except for the value at r = 0 the results match with the exact solution for both pinned and clamped plates.

Fig. 6 shows the center deflection w(0) and rotation -dw/dr at r = 0.5265R as functions of the power-law index n for the pinned and clamped circular plates. We note that the rate of increase of the deflection has two different regions; the first region has a rapid increase of the deflection while the second region is marked with a relatively slow increase. This is primarily because of the fact that the coupling coefficient B_{xx} varies with n rapidly for the smaller values of n followed by a slow decay after n > 3. The rate of increase in the deflection or slope in the second part is less for clamped plates than for the pinned plates. The reason is the fact that the clamped plate is relatively stiffer than the pinned plate.

4.2. Nonlinear analysis

The resulting nonlinear equations after discretization can be solved using either direct iteration or Newton's iteration schemes (see Reddy [32]). It is found that the direct iteration scheme does not converge even after 50 iterations in some cases, especially for FGM plates. On

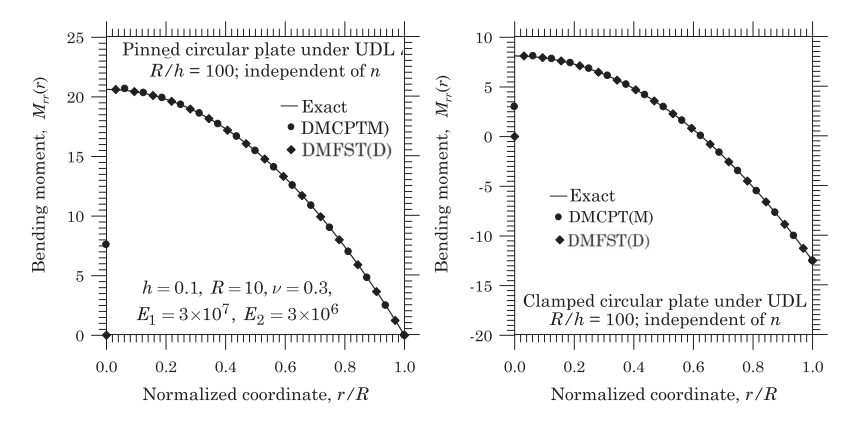


Fig. 5. Plots of the post-computed and nodal values of the bending moment M_{π} of pinned and clamped circular plates as functions of the normalized radial coordinate, r/R. The solid lines correspond to the analytical solutions and symbols to the numerical solutions. The results are independent of the n.

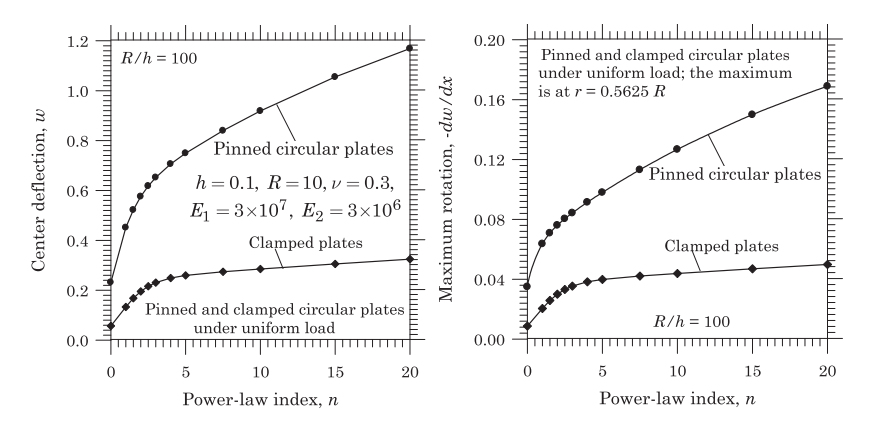


Fig. 6. Plots of the center deflection w(0) and -dw/dr at r=0.5625R of pinned and clamped circular plates as a function of the power-law index, n.

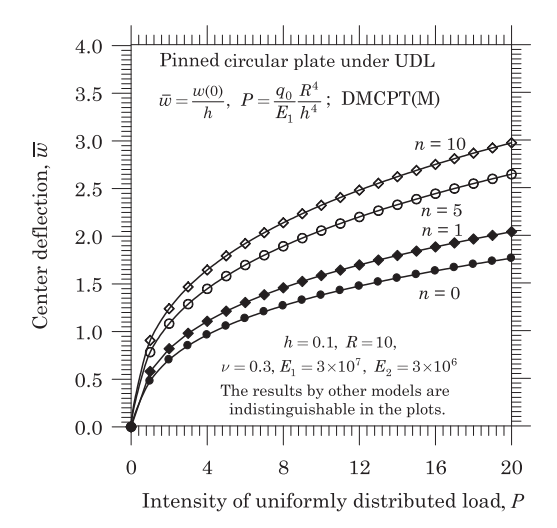


Fig. 7. Plots of the normalized center deflection $\bar{w}=w(0)/h$ versus the load parameter $P=q_0R^4/E_1h^4$ for pinned circular plates, for various value of the power-law index, n.

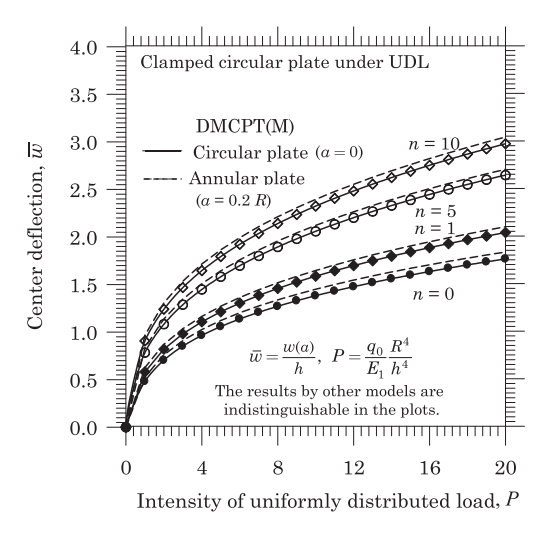


Fig. 9. Plots of the normalized deflection $\bar{w} = w(a)/h$ versus the load parameter $P = q_0 R^4 / E_1 h^4$ for pinned (at the outer rim) annular plates, for various value of the power-law index, n; a = 0 for solid circular plates and a = 0.2R for annular plates.

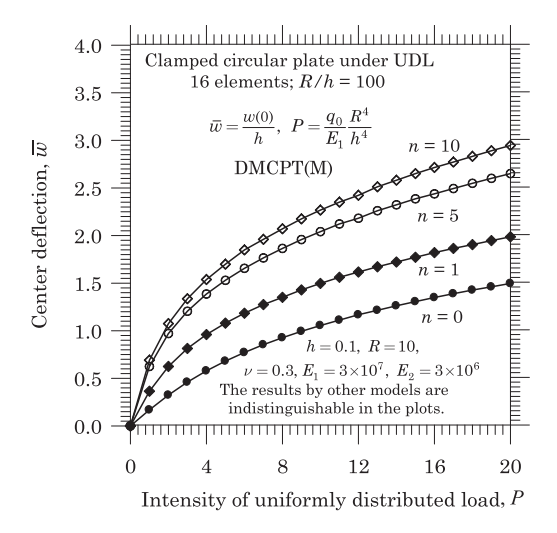


Fig. 8. Plots of the normalized center deflection $\bar{w} = w(0)/h$ versus the load parameter $P = q_0 R^4/E_1 h^4$ for clamped circular plates, for various value of the power-law index, n.

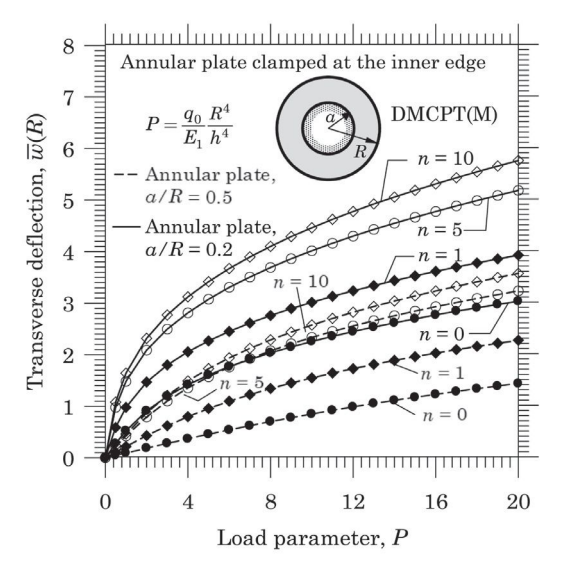


Fig. 10. Plots of the normalized deflection $\bar{w} = w(R)/h$ versus the load parameter $P = q_0 R^4 / E_1 h^4$ for annular plates clamped at the inner edge (r = a, a = 0.2R, 0.5R), for various value of the power-law index, n.

the other hand, the Newton iteration scheme converges for less than 10 iterations (most often for less than 4 iterations). The Newton iteration scheme requires the calculation of the so-called tangent coefficient matrix, which is the sum of the original matrix and their derivatives with respect to the nodal values $\Delta_i^2 = w_i$. A detailed calculation for the FEM models is presented in [32]. The same ideas are used in the DMCDM to compute the tangent matrix coefficients.

Load increments of $\Delta q_0=1.0$ lb/in (175 N/m) and a tolerance of $\varepsilon=10^{-3}$ are used in the nonlinear analysis. The initial solution vector is chosen to be $\Delta^0=\mathbf{0}$ so that the first iteration of the first load step yields the linear solution. The direct iteration scheme does not converge in most cases unless an acceleration parameter, β , is used to evaluate the stiffness matrix, $\mathbf{K}^r=\mathbf{K}(\bar{\Delta}^r)$, at each iteration:

$$\bar{\Delta}^r = (1 - \beta)\Delta^r + \beta\Delta^{r-1}, \quad 0 \le \beta \le 1 \tag{50}$$

where r denotes the iteration number. Thus, using a weighted average of the last two iteration solutions to update the stiffness matrix accelerates the convergence. In the present case, a value of $\beta=0.25$ –0.35 is used (after some study with varying β , starting with $\beta=0$). In some cases, even this strategy does not help to achieve convergence, forcing us to use the Newton iteration scheme.

The nonlinear analysis results for deflections and bending moment obtained by various models are also indistinguishable in the graphs of dimensionless center deflection, $\bar{w}=w(0)/h$ versus the load parameter, $P=q_0R^4/E_1h^4$, as shown in Figs. 7 and 8 for pinned and clamped plates, respectively. The dual mesh control domain method gives essentially the same results as the finite element method, except that the former method has less computational effort due to the computation of the global stiffness matrix and force vector directly, without computing local matrices and assembling.

Plots of the normalized deflection versus the load parameter $\bar{w} = w(a)/h$ versus the load parameter $P = q_0 R^4 / E_1 h^4$ for pinned (at the outer rim) annular plates (a = 0.2R) are presented in Fig. 9; again, all models yield solutions that are indistinguishable in the graphs. The deflections of the annular plates will be higher than the solid circular plates due to the fact that annular plates have less stiffness compared to the solid circular plates for the same boundary conditions. The difference between the deflections of annular plates and solid plates is bigger than that is shown in the plots because the deflections of the solid circular plates (shown in solid lines) are at the center of the plate while those of the annular plate (shown in broken lines) are at r/R = 0.2. Finally, Fig. 10 contains plots of the normalized deflection $\bar{w} = w(R)/h$ for annular plates with internal edge clamped. As the internal radius of the annular plate increases from a = 0.2R to a = 0.5R, the deflection of the outer edge decreases substantially because of the reduction in free span of the plate.

5. Summary and conclusions

In this paper the classical (CPT) and first-order (FSDT) plate theories for axisymmetric bending of circular plates, accounting for through-thickness power-law variation of a two-constituent material and the von Kármán nonlinear strains, are presented, and mixed and displacement models using the dual mesh finite domain are created. Numerical results are presented for pinned and clamped solid circular and pinned annular plates, showing the effect of the power-law index on the load–deflection behavior. In all cases, the results predicted by all computational models gave essentially the same results.

With the developed programs for the five models presented here, a number of other problems with a variety of boundary conditions may be analyzed. For example, circular plates with spring (extensional as well as torsional) supports and annular plates with a combination of boundary conditions at the inner and outer edges, and for different material distributions, can be readily analyzed. Extension of the DMCDM method to problems of plane elasticity, plate bending, coupled elasticity and diffusion (thermal and moisture) and others are waiting attention.

Declaration of Competing Interest

The authors declare that they have no known competing financial interests or personal relationships that could have appeared to influence the work reported in this paper.

Acknowledgments

The first two authors gratefully acknowledge the support of this research by Technical Data Analysis (TDA) grant and National Science Foundation award 1952873 to Texas A&M University.

Appendix A. Appendix A

A.1. The mixed model of the CPT

The following formulas are used in the development of the discretized equations (see Nampally and Reddy [29]):

$$[u(r)]_{r_{l}^{(l)}}^{r_{l}^{(l)}} = \frac{1}{2}(U_{l+1} - U_{l-1})$$
(51a)

$$[u(r)]_{r=0.5h_1} = \frac{1}{2}(U_1 + U_2), \qquad [u(r)]_{r=R-0.5h_N} = \frac{1}{2}(U_N + U_{N+1})$$
 (51b)

$$\left[r\frac{du}{dr}\right]_{r^{(I)}}^{r^{(I)}_{B}} = \left(\frac{r_{A}^{(I)}}{h_{I-1}}\right)U_{I-1} - \left(\frac{r_{A}^{(I)}}{h_{I-1}} + \frac{r_{B}^{(I)}}{h_{I}}\right)U_{I} + \left(\frac{r_{B}^{(I)}}{h_{I}}\right)U_{I+1}$$
(51c)

$$\left[r\frac{du}{dr}\right]_{r=0.5h_1} = \frac{1}{2}(U_2 - U_1), \qquad \left[r\frac{du}{dr}\right]_{r=R-0.5h_N} = \frac{(R-0.5h_N)}{h_N}(U_{N+1} - U_N)$$

(51d)

$$[ru(r)]_{r_A^{(I)}}^{r_B^{(I)}} = -\left(\frac{r_A^{(I)}}{2}\right)U_{I-1} + \left(\frac{r_B^{(I)} - r_A^{(I)}}{2}\right)U_I + \left(\frac{r_B^{(I)}}{2}\right)U_{I+1}$$
 (51e)

$$[ru(r)]_{r=0.5h_1} = \frac{h_1}{4}(U_1 + U_2), \qquad [ru(r)]_{r=R-0.5h_N} = \frac{(R-0.5h_N)}{2}(U_{N+1} + U_N)$$

(51f)

$$\left[r^{2}u(r)\right]_{r_{A}^{(I)}}^{r_{B}^{(I)}} = -\frac{r_{A}^{(I)^{2}}}{2}U_{I-1} + \left(\frac{r_{B}^{(I)^{2}} - r_{A}^{(I)^{2}}}{2}\right)U_{I} + \frac{r_{B}^{(I)^{2}}}{2}U_{I+1}$$
 (51g)

$$[r^2u(r)]_{r=0.5h_1}=\frac{h_1^2}{8}(U_1+U_2),$$

$$[r^{2}u(r)]_{r=R-0.5h_{N}} = \frac{(R-0.5h_{N})^{2}}{2}(U_{N}+U_{N+1})$$
 (51h)

$$\left[r^{2}\frac{du}{dr}\right]_{r_{B}^{(I)}}^{r_{B}^{(I)}} = \frac{r_{A}^{(I)^{2}}}{h_{I-1}}U_{I-1} - \left(\frac{r_{B}^{(I)^{2}}}{h_{I}} + \frac{r_{A}^{(I)^{2}}}{h_{I-1}}\right)U_{I} + \frac{r_{B}^{(I)^{2}}}{h_{I}}U_{I+1}$$
(51i)

$$\left[r^2 rac{du}{dr}
ight]_{r=0.5h_1} = rac{h_1}{4}(U_2 - U_1),$$

$$\left[r^{2}\frac{du}{dr}\right]_{r=R-0.5h_{N}} = \frac{\left(R-0.5h_{N}\right)^{2}}{h_{N}}\left(U_{N+1}-U_{N}\right) \tag{51j}$$

The stiffness coefficients are defined by

$$\begin{split} & K_{l-3}^{l} = \overline{A} \left[r \frac{d \psi_{l}^{(l-1)}}{dr} + \nu \psi_{l}^{(l-1)} \right]_{r=r_{A}^{(l)}} + \overline{A} \int_{r_{A}^{(l)}}^{r_{l}} \left(\nu \frac{d \psi_{l}^{(l-1)}}{dr} + \frac{1}{r} \psi_{l}^{(l-1)} \right) dr \\ & + \overline{B} B (1 - \nu^{2}) \int_{r_{A}}^{r_{l}} \frac{1}{r} \psi_{l}^{(l-1)} dr \\ & K_{l}^{l} = \overline{A} \left[r \frac{d \psi_{l}^{(l-1)}}{dr} + \nu \psi_{l}^{(l-1)} \right]_{r=r_{A}^{(l)}} + \overline{A} \int_{r_{A}^{(l)}}^{r_{l}} \left(\nu \frac{d \psi_{l}^{(l)}}{dr} + \frac{1}{r} \psi_{l}^{(l-1)} \right) dr \\ & + \overline{B} B (1 - \nu^{2}) \int_{r_{A}^{(l)}}^{r_{l}} \frac{1}{r} \psi_{l}^{(l-1)} dr - \overline{A} \left[r \frac{d \psi_{l}^{(l)}}{dr} + \nu \psi_{l}^{(l)} \right]_{r=r_{A}^{(l)}} + \overline{A} \int_{r_{A}^{(l)}}^{r_{B}} \left(\nu \frac{d \psi_{l}^{(l)}}{dr} + \nu \psi_{l}^{(l)} \right) dr \\ & + \overline{A} \int_{r_{A}^{(l)}}^{r_{B}^{(l)}} \left(\nu \frac{d \psi_{l}^{(l)}}{dr} + \frac{1}{r} \psi_{l}^{(l)} \right) dr + \overline{B} B (1 - \nu^{2}) \int_{r_{A}^{(l)}}^{r_{B}^{(l)}} \frac{1}{r} \psi_{l}^{(l)} dr \\ & + \overline{A} B (1 - \nu^{2}) \int_{r_{A}^{(l)}}^{r_{B}^{(l)}} \frac{1}{r} \psi_{l}^{(l)} dr \\ & + \overline{B} B (1 - \nu^{2}) \int_{r_{A}^{(l)}}^{r_{B}^{(l)}} \frac{1}{r} \psi_{l}^{(l)} dr \\ & + \overline{B} B (1 - \nu^{2}) \int_{r_{A}^{(l)}}^{r_{B}^{(l)}} \frac{1}{r} \psi_{l}^{(l)} dr \\ & + \overline{B} B (1 - \nu^{2}) \int_{r_{A}^{(l)}}^{r_{B}^{(l)}} \frac{1}{r} \psi_{l}^{(l)} dr \\ & + \overline{B} B (1 - \nu^{2}) \int_{r_{A}^{(l)}}^{r_{B}^{(l)}} \frac{1}{r} \psi_{l}^{(l)} dr \\ & + \overline{B} B (1 - \nu^{2}) \int_{r_{A}^{(l)}}^{r_{B}^{(l)}} \frac{1}{r} \psi_{l}^{(l)} dr \\ & + \overline{B} B (1 - \nu^{2}) \int_{r_{A}^{(l)}}^{r_{B}^{(l)}} \frac{1}{r} \psi_{l}^{(l)} dr \\ & + \overline{B} B (1 - \nu^{2}) \int_{r_{A}^{(l)}}^{r_{B}^{(l)}} \frac{1}{r} \psi_{l}^{(l)} dr \\ & + \overline{B} B (1 - \nu^{2}) \int_{r_{A}^{(l)}}^{r_{B}^{(l)}} \frac{1}{r} \psi_{l}^{(l)} dr \\ & + \overline{B} B (1 - \nu^{2}) \int_{r_{A}^{(l)}}^{r_{B}^{(l)}} \frac{1}{r} \psi_{l}^{(l)} dr \\ & + \overline{B} B (1 - \nu^{2}) \int_{r_{A}^{(l)}}^{r_{B}^{(l)}} \frac{1}{r} \psi_{l}^{(l)} dr \\ & + \overline{B} B (1 - \nu^{2}) \int_{r_{A}^{(l)}}^{r_{B}^{(l)}} \frac{1}{r} \psi_{l}^{(l)} dr \\ & + \overline{B} B (1 - \nu^{2}) \int_{r_{A}^{(l)}}^{r_{A}^{(l)}} \frac{1}{r} \psi_{l}^{(l)} dr \\ & + \overline{B} B (1 - \nu^{2}) \int_{r_{A}^{(l)}}^{r_{A}^{(l)}} \frac{1}{r} \psi_{l}^{(l)} dr \\ & + \overline{B} B (1 - \nu^{2}) \int_{r_{A}^{(l)}}^{r_{A}^{(l)}} \frac{1}{r} \psi_{l}^{(l)} dr \\ & + \overline{B} B (1 - \nu^{2}) \int_{r_{A}^{(l)}}^{r_{A}^{(l)}} \frac{1}{r} \psi_{$$

$$\begin{split} & K_{I+1}^{I+1} = -\left[r\frac{dw_{2}^{(J)}}{dr} + (1-\nu)\psi_{2}^{(J)} + \overline{B}r\delta W_{J}\psi_{2}^{(J)}\right]_{r=r_{B}^{(I)}} \\ & K_{I-3}^{I+2} = \overline{B}\int_{r_{A}^{(I)}}^{r_{I}} \left[r\frac{dw_{1}^{(J-1)}}{dr} + \nu\psi_{1}^{(J-1)}\right] dr \\ & K_{I}^{I+2} = \overline{B}\int_{r_{A}^{(I)}}^{r_{I}} \left[r\frac{dw_{2}^{(J-1)}}{dr} + \nu\psi_{2}^{(J-1)}\right] dr + \overline{B}\int_{r_{I}}^{r_{B}^{(I)}} \left[r\frac{dw_{1}^{(J)}}{dr} + \nu\psi_{1}^{(J)}\right] dr \\ & K_{I+3}^{I+2} = \overline{B}\int_{r_{I}}^{r_{B}^{(I)}} \left[r\frac{dw_{2}^{(J)}}{dr} + \nu\psi_{2}^{(J)}\right] dr \\ & K_{I+2}^{I+2} = \left[r\frac{dw_{1}^{(J-1)}}{dr}\right]_{r=r_{A}^{(I)}} + \int_{r_{A}^{(I)}}^{r_{I}} \left[(1-\nu)\frac{dw_{1}^{(J-1)}}{dr} + \frac{1}{2}\overline{B}r\delta W_{J-1}\frac{dw_{1}^{(J-1)}}{dr}\right] dr \\ & K_{I+1}^{I+2} = \left[r\frac{dw_{2}^{(J-1)}}{dr}\right]_{r=r_{A}^{(I)}} + \int_{r_{A}^{(I)}}^{r_{B}} \left[(1-\nu)\frac{dw_{1}^{(J)}}{dr} + \frac{1}{2}\overline{B}r\delta W_{J}\frac{dw_{2}^{(J-1)}}{dr}\right] dr \\ & - \left[r\frac{dw_{1}^{(J)}}{dr}\right]_{r=r_{B}^{(I)}} + \int_{r_{I}}^{r_{B}^{(I)}} \left[(1-\nu)\frac{dw_{1}^{(J)}}{dr} + \frac{1}{2}\overline{B}r\delta W_{J}\frac{dw_{2}^{(J)}}{dr}\right] dr \\ & K_{I+4}^{I+2} = -\left[r\frac{dw_{2}^{(J)}}{dr}\right]_{r=r_{B}^{(I)}} + K_{I+5}^{r_{B}^{(I)}} \left[(1-\nu)\frac{dw_{2}^{(J)}}{dr} + \frac{1}{2}\overline{B}r\delta W_{J}\frac{dw_{2}^{(J)}}{dr}\right] dr \\ & K_{I+2}^{I+2} = -\frac{1}{D}\int_{r_{A}^{(I)}}^{r_{I}} r\psi_{1}^{(J-1)} dr, \quad K_{I+5}^{I+2} = -\frac{1}{D}\int_{r_{I}}^{r_{B}^{(I)}} r\psi_{2}^{(J)} dr \\ & K_{I+2}^{I+2} = -\frac{1}{D}\left(\int_{r_{A}^{(I)}}^{r_{I}} r\psi_{1}^{(J-1)} dr + \int_{r_{I}}^{r_{B}^{(I)}} r\psi_{1}^{(J)} dr\right) \\ & F^{I+1} = \int_{r_{A}^{(I)}}^{r_{I}} rq(r) dr + \int_{r_{I}}^{r_{B}^{(I)}} rq(r) dr \end{aligned}$$

Here the superscripts and subscripts (J-1) and J $(J=2,3,\ldots,N)$ refer to the element numbers on the left and right, respectively, of the node number J. The coefficients appearing in the node 1 equations are

$$\begin{split} K_1^1 &= -\overline{A} \left[r \frac{d \psi_1^{(1)}}{dr} + \nu \psi_1^{(1)} \right]_{r=0.5h_1} + \overline{A} \int_0^{0.5h_1} \left(\nu \frac{d \psi_1^{(1)}}{dr} + \frac{1}{r} \psi_1^{(1)} \right) dr \\ &+ \overline{B} B (1 - \nu^2) \int_0^{0.5h_1} \frac{1}{r} \psi_1^{(1)} dr \\ K_4^1 &= -\overline{A} \left[r \frac{d \psi_2^{(1)}}{dr} + \nu \psi_1^{(1)} \right]_{r=0.5h_1} + \overline{A} \int_0^{0.5h_1} \left(\nu \frac{d \psi_2^{(1)}}{dr} + \frac{1}{r} \psi_2^{(1)} \right) dr \\ &+ \overline{B} B (1 - \nu^2) \int_0^{0.5h_1} \frac{1}{r} \psi_2^{(1)} dr \\ K_2^1 &= -\frac{1}{2} \overline{A} \left[r \delta W \frac{d \psi_1^{(1)}}{dr} \right]_{r=0.5h_1} + \frac{\nu}{2} \overline{A} \int_0^{0.5h_1} \delta W \frac{d \psi_1^{(1)}}{dr} dr \\ &- B (1 - \nu^2) \int_0^{0.5h_1} \frac{1}{r} \frac{d \psi_1^{(1)}}{dr} dr \\ K_5^1 &= -\frac{1}{2} \overline{A} \left[r \delta W \frac{d \psi_2^{(1)}}{dr} \right]_{r=0.5h_1} + \frac{\nu}{2} \overline{A} \int_0^{0.5h_1} \delta W \frac{d \psi_2^{(1)}}{dr} dr \\ &- B (1 - \nu^2) \int_0^{0.5h_1} \frac{1}{r} \frac{d \psi_2^{(1)}}{dr} dr \\ K_3^1 &= -\overline{B} \left\{ \left[r \psi_1^{(1)} \right]_{r=0.5h_1} + \nu \int_0^{0.5h_1} \psi_1^{(1)} dr \right\} \\ K_6^2 &= -\overline{B} \left\{ \left[r \psi_1^{(1)} \right]_{r=0.5h_1} + \nu \int_0^{0.5h_1} \psi_1^{(1)} dr \right\} \\ K_7^2 &= (1 - \nu^2) D \overline{B} \left[\frac{1}{r} \psi_1^{(1)} \right]_{r=0.5h_1} - \overline{A} \left[\delta W \left(r \frac{d \psi_1^{(1)}}{dr} + \nu \psi_1^{(1)} \right) \right]_{r=0.5h_1} \\ K_7^2 &= -(1 - \nu^2) D \left[\frac{1}{r} \frac{d \psi_1^{(1)}}{dr} \right]_{r=0.5h_1} - \overline{A} \left[(\delta W)^2 r \frac{d \psi_1^{(1)}}{dr} \right]_{r=0.5h_1} \\ K_8^2 &= -\left[r \frac{d \psi_1^{(1)}}{dr} + (1 - \nu) \psi_1^{(1)} + \overline{B} r \delta W \psi_1^{(1)} \right]_{r=0.5h_1} \\ K_8^2 &= -\left[r \frac{d \psi_2^{(1)}}{dr} + (1 - \nu) \psi_1^{(1)} + \overline{B} r \delta W \psi_1^{(1)} \right]_{r=0.5h_1} \\ K_6^2 &= -\left[r \frac{d \psi_2^{(1)}}{dr} + (1 - \nu) \psi_1^{(1)} + \overline{B} r \delta W \psi_2^{(1)} \right]_{r=0.5h_1} \\ K_6^2 &= -\left[r \frac{d \psi_2^{(1)}}{dr} + (1 - \nu) \psi_1^{(1)} + \overline{B} r \delta W \psi_2^{(1)} \right]_{r=0.5h_1} \\ K_9^2 &= -\left[r \frac{d \psi_2^{(1)}}{dr} + (1 - \nu) \psi_1^{(1)} + \overline{B} r \delta W \psi_2^{(1)} \right]_{r=0.5h_1} \\ K_9^2 &= -\left[r \frac{d \psi_2^{(1)}}{dr} + (1 - \nu) \psi_1^{(1)} + \overline{B} r \delta W \psi_2^{(1)} \right]_{r=0.5h_1} \\ K_9^2 &= -\left[r \frac{d \psi_2^{(1)}}{dr} + (1 - \nu) \psi_1^{(1)} + \overline{B} r \delta W \psi_2^{(1)} \right]_{r=0.5h_1} \\ K_9^2 &= -\left[r \frac{d \psi_2^{(1)}}{dr} + (1 - \nu) \psi_1^{(1)} + \overline{B} r \delta W \psi_2^{(1)} \right]_{r=0.5h_1} \\ K_9^2 &= -\left[r \frac{d \psi_2^{(1)}}{dr} + (1 - \nu) \psi_2^{(1)} + \overline{B} r \delta W \psi_2^{(1)} \right]_{r=0.5h_1} \\ K_9^2 &= -\left[r \frac{d \psi_2^{(1)}}{dr} +$$

$$\begin{split} K_{1}^{3} &= \overline{B} \int_{0}^{0.5h_{1}} \left[r \frac{d \psi_{1}^{(1)}}{dr} + \nu \psi_{1}^{(1)} \right] dr, \quad K_{4}^{3} &= \overline{B} \int_{0}^{0.5h_{1}} \left[r \frac{d \psi_{2}^{(1)}}{dr} + \nu \psi_{2}^{(1)} \right] dr \\ K_{2}^{3} &= - \left[r \frac{d \psi_{1}^{(1)}}{dr} \right]_{r=0.5h_{1}} + \int_{0}^{0.5h_{1}} \left[(1 - \nu) \frac{d \psi_{1}^{(1)}}{dr} + \frac{1}{2} \overline{B} r \delta W \frac{d \psi_{1}^{(1)}}{dr} \right] dr \\ K_{5}^{3} &= \left[r \frac{d \psi_{2}^{(1)}}{dr} \right]_{r=0.5h_{1}} + \int_{0}^{0.5h_{1}} \left[(1 - \nu) \frac{d \psi_{2}^{(1)}}{dr} + \frac{1}{2} \overline{B} r \delta W \frac{d \psi_{2}^{(1)}}{dr} \right] dr \\ K_{3}^{3} &= -\frac{1}{D} \int_{0}^{0.5h_{1}} r \psi_{1}^{(1)} dr, \quad K_{6}^{3} &= -\frac{1}{D} \int_{0}^{0.5h_{1}} r \psi_{2}^{(1)} dr \\ F^{2} &= \int_{0}^{0.5h_{1}} r q(r) dr + \int_{0}^{0.5h_{1}} r q(r) dr, \quad \delta W &= \frac{W_{2} - W_{1}}{h_{1}} \end{split}$$

Similar expressions for node N + 1 can be written.

A.2. The displacement model of the FSDT

The stiffness coefficients of the displacement model of the FSDT are

$$\begin{split} & K_{l-3}^{l} = A \left[r \frac{d \varphi_{l}^{(l-1)}}{dr} + \nu \psi_{1}^{(l-1)} \right]_{r=r_{A}^{(l)}} + A \int_{r_{A}^{(l)}}^{r_{I}} \left(\nu \frac{d \varphi_{l}^{(l-1)}}{dr} + \frac{1}{r} \psi_{1}^{(l-1)} \right) dr \\ & K_{l}^{l} = A \left[r \frac{d \varphi_{l}^{(l)}}{dr} + \nu \psi_{1}^{(l-1)} \right]_{r=r_{A}^{(l)}} + A \int_{r_{A}^{(l)}}^{r_{I}} \left(\nu \frac{d \varphi_{l}^{(l)}}{dr} + \frac{1}{r} \psi_{1}^{(l-1)} \right) dr \\ & - A \left[r \frac{d \varphi_{l}^{(l)}}{dr} + \nu \psi_{1}^{(l)} \right]_{r=r_{B}^{(l)}} + A \int_{r_{I}^{(l)}}^{r_{I}} \left(\nu \frac{d \varphi_{l}^{(l)}}{dr} + \frac{1}{r} \psi_{1}^{(l)} \right) dr \\ & K_{l+3}^{l} = - A \left[r \frac{d \varphi_{l}^{(l)}}{dr} + \nu \psi_{1}^{(l)} \right]_{r=r_{B}^{(l)}} + A \int_{r_{A}^{(l)}}^{r_{I}} \left(\nu \frac{d \varphi_{l}^{(l)}}{dr} + \frac{1}{r} \psi_{1}^{(l)} \right) dr \\ & K_{l+1}^{l} = \frac{1}{2} A \left[r \delta W_{J-1} \frac{d \varphi_{l}^{(l-1)}}{dr} \right]_{r=r_{A}^{(l)}} + \frac{\nu}{2} A \int_{r_{A}^{(l)}}^{r_{I}} \delta W_{J-1} \frac{d \varphi_{l}^{(l-1)}}{dr} dr \\ & K_{l+1}^{l} = \frac{1}{2} A \left[r \delta W_{J-1} \frac{d \varphi_{l}^{(l-1)}}{dr} \right]_{r=r_{B}^{(l)}} + \frac{\nu}{2} A \int_{r_{A}^{(l)}}^{r_{B}} \delta W_{J} \frac{d \varphi_{l}^{(l)}}{dr} dr \\ & K_{l+1}^{l} = \frac{1}{2} A \left[r \delta W_{J} \frac{d \varphi_{l}^{(l)}}{dr} \right]_{r=r_{B}^{(l)}} + \frac{\nu}{2} A \int_{r_{A}^{(l)}}^{r_{B}} \delta W_{J} \frac{d \varphi_{l}^{(l)}}{dr} dr \\ & K_{l+1}^{l} = \frac{1}{2} A \left[r \delta W_{J} \frac{d \varphi_{l}^{(l)}}{dr} \right]_{r=r_{B}^{(l)}} + \frac{\nu}{2} A \int_{r_{A}^{(l)}}^{r_{B}} \delta W_{J} \frac{d \varphi_{l}^{(l)}}{dr} dr \\ & K_{l+1}^{l} = B \left[r \frac{d \varphi_{l}^{(l-1)}}{dr} + \nu \psi_{1}^{(l-1)} \right]_{r=r_{B}^{(l)}} + B \int_{r_{A}^{(l)}}^{r_{B}} \left(\nu \frac{d \varphi_{l}^{(l)-1}}{dr} + \frac{1}{r} \psi_{1}^{(l-1)} \right) dr \\ & K_{l+2}^{l} = B \left[r \frac{d \varphi_{l}^{(l)-1}}{dr} + \nu \psi_{1}^{(l-1)} \right]_{r=r_{B}^{(l)}} + B \int_{r_{A}^{(l)}}^{r_{B}} \left(\nu \frac{d \varphi_{l}^{(l)-1}}{dr} + \frac{1}{r} \psi_{1}^{(l)} \right) dr \\ & K_{l+3}^{l+1} = A \left[\delta W_{J-1} \left(r \frac{d \varphi_{l}^{(l)-1}}{dr} + \nu \psi_{1}^{(l)-1} \right) \right]_{r=r_{B}^{(l)}} + B \int_{r_{A}^{(l)}}^{r_{B}} \left(\nu \frac{d \varphi_{l}^{(l)-1}}{dr} + \frac{1}{r} \psi_{1}^{(l)} \right) dr \\ & K_{l+3}^{l+1} = A \left[\delta W_{J-1} \left(r \frac{d \varphi_{l}^{(l)-1}}{dr} + \nu \psi_{1}^{(l)} \right) \right]_{r=r_{B}^{(l)}} - A \left[\delta W_{J} \left(r \frac{d \varphi_{l}^{(l)-1}}{dr} + \nu \psi_{1}^{(l)} \right) \right]_{r=r_{B}^{(l)}} \\ & - S_{re} \left[r \frac{d \psi_{l}^{(l)-1}}{dr} \right]_{r=r_{A}^{(l)}} - \frac{1}{2} A \left[$$

$$\begin{split} K_{l+1}^{l+1} &= \left[S_{r2} r \psi_{1}^{(J-1)} + B \delta W_{J-1} \left(r \frac{d \psi_{1}^{(J-1)}}{dr} + \nu \psi_{1}^{(J-1)} \right) \right]_{r=r_{A}^{(I)}} \\ K_{l+2}^{l+1} &= \left[S_{r2} r \psi_{2}^{(J-1)} + B \delta W_{J-1} \left(r \frac{d \psi_{2}^{(J-1)}}{dr} + \nu \psi_{1}^{(J-1)} \right) \right]_{r=r_{A}^{(I)}} \\ &- \left[S_{r2} r \psi_{1}^{(J)} + B \delta W_{J} \left(r \frac{d \psi_{2}^{(J)}}{dr} + \nu \psi_{1}^{(J)} \right) \right]_{r=r_{B}^{(I)}} \\ K_{l+3}^{l+2} &= - \left[S_{r2} r \psi_{2}^{(J)} + B \delta W_{J} \left(r \frac{d \psi_{2}^{(J)}}{dr} + \nu \psi_{2}^{(J)} \right) \right]_{r=r_{B}^{(I)}} \\ K_{l+3}^{l+2} &= B \left[r \frac{d \psi_{1}^{(J-1)}}{dr} + \nu \psi_{1}^{(J-1)} \right]_{r=r_{A}^{(J)}} + B \int_{r_{A}^{(I)}}^{r_{I}} \left(\nu \frac{d \psi_{2}^{(J)-1}}{dr} + \frac{1}{r} \psi_{1}^{(J-1)} \right) dr \\ K_{l}^{l+2} &= B \left[r \frac{d \psi_{1}^{(J-1)}}{dr} + \nu \psi_{1}^{(J-1)} \right]_{r=r_{A}^{(I)}} + B \int_{r_{A}^{(I)}}^{r_{I}} \left(\nu \frac{d \psi_{2}^{(J)-1}}{dr} + \frac{1}{r} \psi_{2}^{(J-1)} \right) dr \\ - B \left[r \frac{d \psi_{1}^{(J)-1}}{dr} + \nu \psi_{1}^{(J)} \right]_{r=r_{A}^{(I)}} + B \int_{r_{A}^{(I)}}^{r_{I}} \left(\nu \frac{d \psi_{2}^{(J)-1}}{dr} + \frac{1}{r} \psi_{2}^{(J)} \right) dr \\ K_{l+3}^{l+2} &= -B \left[r \frac{d \psi_{1}^{(J)-1}}{dr} + \nu \psi_{2}^{(J)} \right]_{r=r_{A}^{(I)}} + B \int_{r_{A}^{(I)}}^{r_{I}} \left(\nu \frac{d \psi_{2}^{(J)-1}}{dr} + \frac{1}{r} \psi_{2}^{(J)} \right) dr \\ K_{l+2}^{l+2} &= \frac{1}{2} B \left[r \delta W_{J-1} \frac{d \psi_{2}^{(J)-1}}{dr} \right]_{r=r_{A}^{(I)}} + \frac{1}{2} B \int_{r_{A}^{(I)}}^{r_{I}} \delta W_{J-1} \frac{d \psi_{2}^{(J)-1}}{dr} dr \\ + S_{r_{A}} \left(J_{A}^{r_{A}} \frac{d \psi_{2}^{(J)-1}}{dr} \right)_{r=r_{B}^{(I)}} + \frac{1}{2} B \int_{r_{A}^{(I)}}^{r_{B}} \delta W_{J} \frac{d \psi_{2}^{(J)}}{dr} dr \\ + S_{r_{A}} \left(J_{A}^{r_{A}} \frac{d \psi_{2}^{(J)-1}}{dr} \right)_{r=r_{B}^{(I)}} + \frac{1}{2} B \int_{r_{A}^{(I)}}^{r_{B}} \delta W_{J} \frac{d \psi_{2}^{(J)}}{dr} dr \\ + S_{r_{A}} \left(J_{A}^{r_{A}} \frac{d \psi_{2}^{(J)-1}}{dr} \right)_{r=r_{B}^{(I)}} + D \int_{r_{A}^{(I)}}^{r_{B}} \left(\nu \frac{d \psi_{2}^{(J)-1}}{dr} + \frac{1}{r} \psi_{1}^{(J)-1} \right) dr \\ + S_{r_{A}} \left(J_{A}^{r_{A}} \psi_{1}^{(J)-1} \right)_{r=r_{B}^{(I)}} + D \int_{r_{A}^{(I)}}^{r_{B}} \left(\nu \frac{d \psi_{2}^{(J)-1}}{dr} + \frac{1}{r} \psi_{1}^{(J)-1} \right) dr \\ + S_{r_{A}} \left(J_{A}^{r_{A}} \psi_{2}^{(J)-1} \right)_{r=r_{B}^{(I)}} + D \int_{r_{A}^{(I)}}^{r_{B}} \left(\nu \frac{d \psi_{2}^{(J)-1}}{dr} + \frac{1}{r} \psi_{1}^{(J)} \right) dr \\ +$$

Here the superscripts and subscripts (J-1) and J $(J=2,3,\ldots,N)$ refer to the element numbers on the left and right, respectively, of the node number J. Node 1 equations are

$$\begin{split} K_1^1 &= -A \left[r \frac{d \psi_1^{(1)}}{dr} + \nu \psi_1^{(1)} \right]_{r=0.5h_1} + A \int_0^{0.5h_1} \left(\nu \frac{d \psi_1^{(1)}}{dr} + \frac{1}{r} \psi_1^{(1)} \right) dr \\ K_4^1 &= -A \left[r \frac{d \psi_2^{(1)}}{dr} + \nu \psi_1^{(1)} \right]_{r=0.5h_1} + A \int_0^{0.5h_1} \left(\nu \frac{d \psi_2^{(1)}}{dr} + \frac{1}{r} \psi_2^{(1)} \right) dr \\ K_2^1 &= -\frac{1}{2} A \left[r \delta W \frac{d \psi_1^{(1)}}{dr} \right]_{r=0.5h_1} + \frac{\nu}{2} A \int_0^{0.5h_1} \delta W \frac{d \psi_1^{(1)}}{dr} dr \\ K_5^1 &= -\frac{1}{2} A \left[r \delta W \frac{d \psi_2^{(1)}}{dr} \right]_{r=0.5h_1} + \frac{\nu}{2} A \int_0^{0.5h_1} \delta W \frac{d \psi_2^{(1)}}{dr} dr \\ K_3^2 &= -B \left[r \frac{d \psi_1^{(1)}}{dr} + \nu \psi_1^{(1)} \right]_{r=0.5h_1} + B \int_0^{0.5h_1} \left(\nu \frac{d \psi_2^{(1)}}{dr} + \frac{1}{r} \psi_1^{(1)} \right) dr \\ K_6^2 &= -B \left[r \frac{d \psi_2^{(1)}}{dr} + \nu \psi_1^{(1)} \right]_{r=0.5h_1} + B \int_0^{0.5h_1} \left(\nu \frac{d \psi_2^{(1)}}{dr} + \frac{1}{r} \psi_2^{(1)} \right) dr \\ K_1^2 &= -A \left[\delta W \left(r \frac{d \psi_1^{(1)}}{dr} + \nu \psi_1^{(1)} \right) \right]_{r=0.5h_1} \\ K_2^2 &= -\left[S_{rx} r \frac{d \psi_1^{(1)}}{dr} + \frac{1}{2} A (\delta W)^2 r \frac{d \psi_2^{(1)}}{dr} \right]_{r=0.5h_1} \\ K_2^2 &= -\left[S_{rx} r \frac{d \psi_2^{(1)}}{dr} + \frac{1}{2} A (\delta W)^2 r \frac{d \psi_2^{(1)}}{dr} \right]_{r=0.5h_1} \\ K_3^2 &= -\left[S_{rx} r \psi_2^{(1)} + B \delta W \left(r \frac{d \psi_2^{(1)}}{dr} + \nu \psi_1^{(1)} \right) \right]_{r=0.5h_1} \\ K_6^2 &= -\left[S_{rx} r \psi_2^{(1)} + B \delta W \left(r \frac{d \psi_2^{(1)}}{dr} + \nu \psi_1^{(1)} \right) \right]_{r=0.5h_1} \\ K_1^3 &= -B \left[r \frac{d \psi_2^{(1)}}{dr} + \nu \psi_1^{(1)} \right]_{r=0.5h_1} + B \int_0^{0.5h_1} \left(\nu \frac{d \psi_2^{(1)}}{dr} + \frac{1}{r} \psi_1^{(1)} \right) dr \\ K_2^3 &= -\frac{1}{2} B \left[r \delta W \frac{d \psi_2^{(1)}}{dr} \right]_{r=0.5h_1} + \frac{\nu}{2} B \int_0^{0.5h_1} \delta W \frac{d \psi_2^{(1)}}{dr} dr \\ K_2^3 &= -\frac{1}{2} B \left[r \delta W \frac{d \psi_2^{(1)}}{dr} \right]_{r=0.5h_1} + \frac{\nu}{2} B \int_0^{0.5h_1} \delta W \frac{d \psi_2^{(1)}}{dr} dr \\ K_3^2 &= -\frac{1}{2} B \left[r \delta W \frac{d \psi_2^{(1)}}{dr} \right]_{r=0.5h_1} + \frac{\nu}{2} B \int_0^{0.5h_1} \delta W \frac{d \psi_2^{(1)}}{dr} dr \\ K_3^2 &= -\frac{1}{2} B \left[r \delta W \frac{d \psi_2^{(1)}}{dr} \right]_{r=0.5h_1} + \frac{\nu}{2} B \int_0^{0.5h_1} \delta W \frac{d \psi_2^{(1)}}{dr} dr \\ K_3^2 &= S_{rx} \int_0^{0.5h_1} \psi_1^{(1)} r dr - D \left[r \frac{d \psi_2^{(1)}}{dr} + \nu \psi_1^{(1)} \right]_{r=0.5h_1} \right]_{r=0.5h_1} \\ + D \int_0^{0.5h_1} \left(\nu \frac{d \psi_2^{(1)}}{dr} \right)_{r=0.5h_1} + \frac{\nu}{2} B \int_0^{0.5h_1} \delta W \frac{d \psi_2^{(1)}}{dr} dr$$

References

 $+D\int_{0}^{0.5h_{1}}\left(
u\frac{d\psi_{2}^{(1)}}{dr}+\frac{1}{r}\psi_{2}^{(1)}
ight)dr$

 $F^2 = \int_0^{0.5h_1} rq(r) dr, \qquad \delta W = \frac{V_2 - W_1}{L}$

- [1] Koizumi M. "The concept of FGM. Ceram Trans Function Grad Mater 1993;34:3–10.
- [2] Praveen GN, Reddy JN. "Nonlinear transient thermoelastic analysis of functionally graded ceramic-metal plates. J Solids Struct 1998;35(,33):4457–76.
- [3] Reddy JN, Chin CD. Thermomechanical analysis of functionally graded cylinders and plates. J Therm Stresses 1998;26(1):593–626.
- [4] Praveen GN, Chin CD, Reddy JN. Thermoelastic analysis of functionally graded ceramic-metal cylinder. J Eng Mech ASCE 1999;125(11):1259–66.
- [5] Reddy JN. "Analysis of functionally graded plates. Int J Numer Methods Eng 2000:47:663–84.

- [6] Reddy JN, Cheng Z-Q. Three-dimensional thermomechanical deformations of functionally graded rectangular plates. Eur J Mech A/Solids 2001;20(5):841–60.
- [7] Reddy JN. Microstructure-dependent couple stress theories of functionally graded beams. J Mech Phys Solids 2011;59:2382–99.
- [8] Reddy JN. A general nonlinear third-order theory of functionally graded plates. Int J Aerosp Lightweight Struct 2011;1(1):1–21.
- [9] Reddy JN, Berry Jessica. Modified couple stress theory of axisymmetric bending of functionally graded circular plates. Compos Struct 2012;94:3664–8.
- [10] Arbind A, Reddy JN. Nonlinear analysis of functionally graded microstructuredependent beams. Compos Struct 2013:98:272–81.
- [11] Arbind A, Reddy JN, Srinivasa A. Modified couple stress-based third-order theory for nonlinear analysis of functionally graded beams. Latin Am J Solids Struct 2014;11:459–87.
- [12] Reddy JN, Romanoff Jani, Loya Jose Antonio. Nonlinear finite element analysis of functionally graded circular plates with modified couple stress theory. Eur J Mech A/Solids Mar-Apr 2016.;56:92–104.
- [13] Kim J, Paulino GH. Finite element evaluation of mixed mode stress intensity factors in functionally graded materials. Int J Numer Methods Eng 2002;53:1903-35.
- [14] Zhang Ch, Savaidis A, Savaidis G, Zhu H. Transient dynamic analysis of a cracked functionally graded material by a BIEM. Comput Mater Sci 2003;26:167–74.
- [15] Lü CF, Lim CW, Chen WQ. Size-dependent elastic behavior of FGM ultra-thin films based on generalized refined theory. Int J Solids Struct 2009;46:1176–85.
- [16] Kahrobaiyan MH, Asghari M, Rahaeifard M, Ahmadian MT. Investigation of the size-dependent dynamic characteristics of atomic force microscope microcantilevers based on the modified couple stress theory. Int J Eng Sci 2010;48:1985–94.
- [17] Zhang J, Fu Y. "Pull-in analysis of electrically actuated viscoelastic microbeams based on a modified couple stress theory. Meccanica 2012;47:1649–58.
- [18] Shariat BS, Liu Y, Rio G. "Modelling and experimental investigation of geometrically graded NiTi shape memory alloys. Smart Mater Struct 2013;22:025030.
- [19] Li X, Bhushan B, Takashima K, Baek CW, Kim YK. Mechanical characterization of micro/nanoscale structures for MEMS/NEMS applications using nanoindentation techniques. Ultramicroscopy 2003;97:481–94.
- [20] Pei J, Tian F, Thundat T. Glucose biosensor based on the microcantilever. Anal Che 76:2004:292–29..
- [21] Reddy JN. An introduction to the finite element method. 4th ed. New York, NY: McGraw-Hill; 2019.
- [22] Reddy JN. Energy principles and variational methods in applied mechanics. 3rd ed. New York, NY: John Wiley & Sons; 2017.
- [23] Versteeg HK, Malalasekera W. Computational fluid dynamics, the finite volume method, 2nd ed., Pearson Education (Prentice-Hall), Harlow, England, UK; 2007..
- [24] Mazumder S. Numerical methods for partial differential equations. Finite difference and finite volume methods. New York, NY: Elsevier; 2016.
- [25] Reddy JN, Anand NK, Roy P. The finite element and finite volume methods in heat transfer and fluid mechanics, in preparation..
- [26] Reddy JN. A dual mesh finite domain method for the numerical solution of differential equations. Int J Comput Methods Eng Sci Mech 2019;20:212–28.
- [27] Reddy JN, Praneeth Nampally. A dual mesh finite domain method for the analysis of functionally graded beams. Compos Struct 251:2020; Article 112648..
- [28] Reddy JN, Nampally Praneeth, Srinivasa AR. Nonlinear analysis of functionally graded beams using the dual mesh finite domain method and the finite element method. Int J Non-Linear Mech Dec 2020;127:103575.
- [29] Praneeth Nampally, Reddy JN. Bending analysis of functionally graded axisymmetric circular plates using the dual mesh finite domain method. Latin Am J Solid Mech Accepted for publication. doi: 10.1590/1679-78256218..
- [30] Reddy JN, Praneeth Nampally, Martinez. A novel numerical method for the solution of nonlinear equations with applications to heat transfer. Int J Numer Methods Heat Fluid Flow Accepted for publication..
- [31] Reddy JN, Namhee Kim Matthew Martinez. A dual mesh control domain method for the solution of nonlinear poisson's equation and the Navier-Stokes equations for incompressible fluids. Phys Fluids 32:2020;093608. Published online. https://doi.org/10.1063/5.002627.
- [32] Reddy JN. An introduction to nonlinear finite element analysis. 2nd ed. Oxford, UK: Oxford University Press; 2015.
- [33] Wang CM, Reddy JN, Lee KH. Shear deformable beams and plates, relationships with classical solutions. Amsterdam: Elsevier; 2000.
- [34] Reddy JN, Wang CM, Kitipornchai S. Axisymmetric bending of functionally graded circular and annular plates. Eur J Mech 1999;18:185–99.
- [35] Reddy JN. Energy principles and variational methods in applied mechanics. 3rd ed. New York, NY: John Wiley & Sons; 2017.
- [36] Reddy JN. Theory and analysis of plates and shells. 2nd ed. Boca Raton, FL: CRC Press: 2007.

(55)